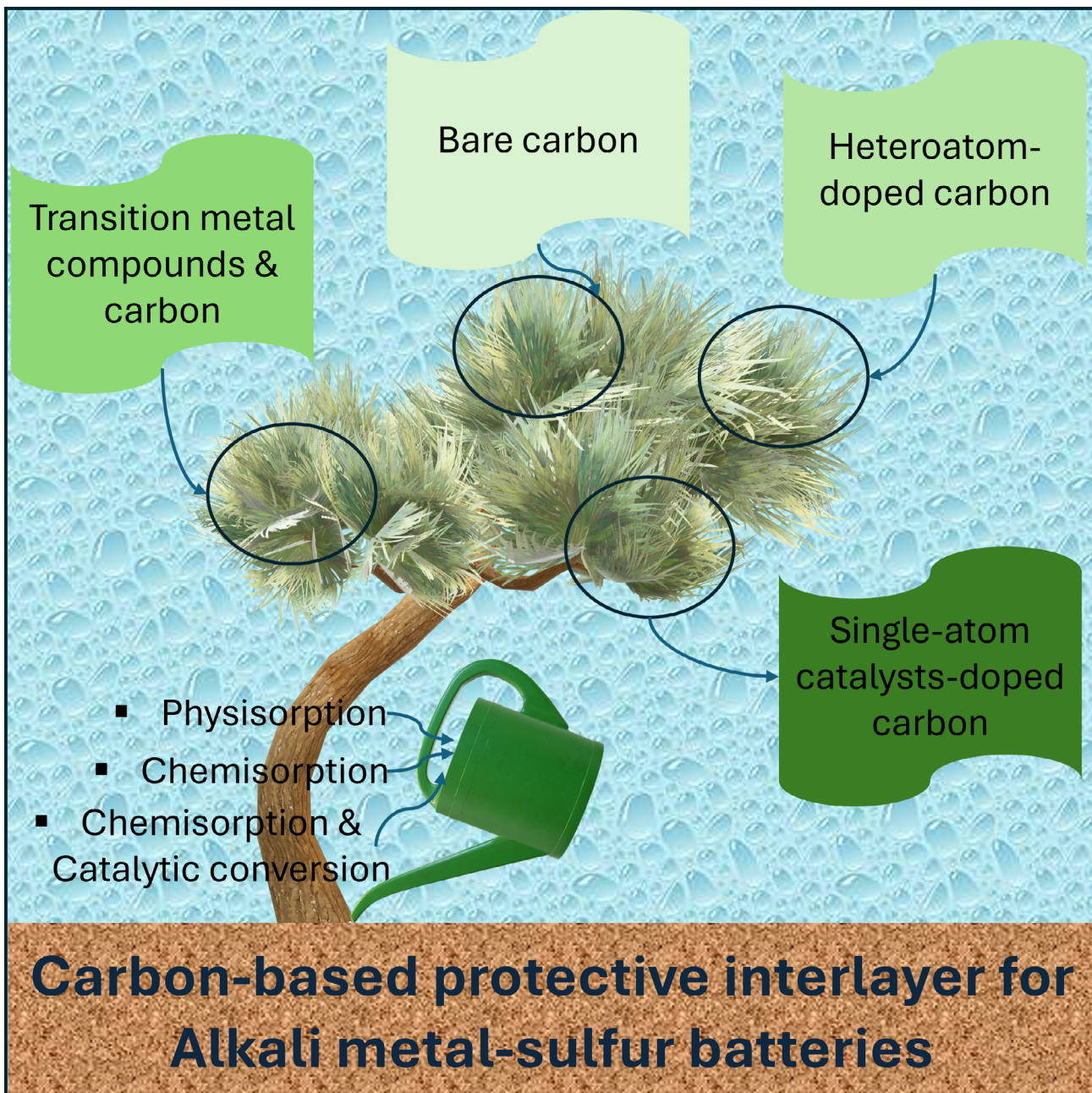


Mechanistic Progress and Challenges for Carbon-Based Protective Interlayer/Separator Modification for the Practical Development of Next-Generation Alkali Metal–Sulfur Batteries

Vikram Kishore Bharti,* Ashish Priyam Goswami, Mudrika Khandelwal,
and Chandra Shekhar Sharma*



Alkali metal–sulfur batteries (AMSBs) are promising for next-generation energy storage, offering much higher energy density than lithium-ion batteries. However, commercialization faces challenges like sulfur's insulating nature, volume expansion, and the polysulfide shuttle effect, which causes poor cycle life, low efficiency, and active material loss. While conductive, porous sulfur hosts help with insulation and volume changes, polysulfide shuttling remains a major issue. A practical solution is adding an interlayer between the cathode and separator, which acts as a physical barrier, an upper current collector, and a polysulfide reservoir, improving electrochemical performance. Though

well-studied in lithium-sulfur batteries, interlayers have received less attention in broader AMSB chemistries. This review examines interlayer roles, fabrication methods, and mechanisms in AMSBs, offering insights into material selection based on different cathode chemistries. Potential limitations in cell assembly are also discussed, and guidelines for optimizing interlayer design are provided. Drawing from our AMSB experience, this study aims to highlight strategies to enhance battery performance. This study hopes this mini-review contributes to advancing AMSBs, paving the way for next-generation battery technologies.

1. Introduction to Alkali Metal–Sulfur Batteries (Metal = Li, K, Na)

Electrochemical energy storage systems are becoming increasingly important across a variety of applications, from portable electronic devices and the latest electric vehicles to the efficient incorporation of intermittent renewable energy sources like solar and wind into smart grids.^[1–3] Since their successful introduction in 1991, lithium-ion batteries (LIBs), which utilize lithium intercalation electrochemistry, have revolutionized the world of portable electronics and nowadays extensively in electrifying vehicles.^[1,4,5] Reliability, stable performance, and the mature techniques for battery assembly are the two major factors that make LIB technology the potential candidate to dominate energy storage solutions.^[4,6–10] Continuous improvements have pushed the energy density of LIBs toward their theoretical maximum. However, this limit remains insufficient to meet the demands of future key markets, such as the widespread electrification of vehicles and the reliable power supply for stationary grid energy storage.^[11–14] On the other hand, LIB requires relatively high fabrication costs owing to the limited specific capacity of cathodic material, uneven distribution of lithium on the earth's crust, and involvement of precious metals.^[4] In addition, the cathode fabrication cost is also higher due to the participation of precious metals.^[15–17] These factors hinder its implementation for large-scale energy storage.^[18,19] Therefore, different battery chemistries must be employed to minimize the flaws of LIBs and require low fabrication costs.

For this endeavor, sulfur-based battery technology seems promising for large-scale energy storage applications owing to

sulfur's high natural abundance, desirable multielectron conversion chemistry, and high theoretical capacity (1675 mA h g^{-1}).^[20] The natural abundance and environmental friendliness of sulfur cathode when clubbed with lithium anode make lithium–sulfur batteries (LSBs) a potential next-generation energy-storage solution.^[21] In addition, having similar chemical properties to lithium, the elements from group one of the periodic table, sodium (Na) and potassium (K), can be coupled with the sulfur cathode to develop alkali metal–sulfur batteries (AMSBs) with great features surpassing LIB technology.^[22] The significant difference lies in the electrochemical reaction mechanism of LIBs and AMSBs. Briefly, AMSBs work on the alloy formation (M_2S , M = Li, K, Na) with a multistep (typically two-step) redox reaction, whereas LIBs are based on Li^+ intercalation/deintercalation. AMSBs are recognized as promising candidates for next-generation electrochemical energy storage systems because of their low cost, high theoretical energy density, eco-friendliness, high abundance of sulfur, and two-electron-transfer reaction mechanism.^[23]

Despite that, AMSBs are severely plagued by several key challenges, including insulating sulfur, shuttle effect of soluble polysulfides, volume changes, unstable electrode-electrolyte interface, and dendrite growth.^[21–24] These bottlenecks should be carefully addressed to develop a commercial solution for AMSBs. Considering this, researchers have made various efforts to tackle these challenges, such as using carbon scaffolds to impart conductivity to the insulating sulfur and using a porous host to sustain the volume changes arising during the electrochemical conversion reaction. However, tackling the shuttle effect of soluble polysulfides (the most notorious effect in sulfur chemistry) needs special consideration as this causes inferior cycle life, poor reversibility (resulting in low Coulombic efficiency), and loss of active material (sulfur). Slowly, people started focusing on developing new strategies outside the cathode by modifying the electrolyte, separator, and/or inserting an interlayer to reduce the polysulfide shuttle effect. In this arena, using an interlayer has attained enormous attention in the last few decades in LSBs to boost the electrochemical characteristic.^[25,26] An interlayer is an independent film positioned between the cathode and separator or between the separator and the anode, without being physically bonded to any of these components. Its purpose is to act as an extra functional layer within the battery, strategically placed to enhance performance, stability, and overall efficiency.

V. K. Bharti, A. P. Goswami, C. S. Sharma
Creative & Advanced Research Based on Nanomaterials (CARBON)
Laboratory
Department of Chemical Engineering
Indian Institute of Technology, Hyderabad
Kandi, Sangareddy, Telangana 502285, India
E-mail: vikram2k23@alumni.iith.ac.in
cssharma@che.iith.ac.in

V. K. Bharti, A. P. Goswami, M. Khandelwal
Cellulose & Composites Laboratory
Department of Materials Science and Metallurgical Engineering
Indian Institute of Technology, Hyderabad
Kandi, Sangareddy, Telangana 502285, India

Manthiram et al.^[27,28] demonstrated this straightforward method to enhance both capacity and cycle stability in batteries by placing a porous, conductive carbon interlayer between the cathode and the separator, and this added interlayer helps improve performance by facilitating electron transport, binding the soluble polysulfides, and trapping active material. These interlayers serve as a physical barrier that not only enhances sulfur utilization but also reduces the shuttle effect and protects the anode from severe corrosion due to attack by soluble polysulfides. Consequently, it functions as an upper current collector, a polysulfide reservoir, and a polysulfide converter. Using the interlayer holds great promise in LSB chemistry, while it has remained unexplored or less explored in other AMSBs. The interaction of an interlayer and soluble polysulfide is broadly illustrated in Figure 1.

An effective interlayer in AMSBs should meet several key criteria. First, it must block polysulfide migration, either by repelling them electrostatically or physically obstructing them. At the same time, it should allow metal ions (M^+) to move freely to support efficient charge and discharge. It also helps by reducing metal-polysulfide buildup near the metal anode and can serve as an upper current collector to recover active material. Additionally, it should absorb volume changes from the sulfur cathode to avoid structural damage, integrate all these functions harmoniously, remain flexible during cycling, and be thin enough to simplify battery assembly while maximizing energy density.^[29–32]

To fabricate an interlayer, carbonaceous materials (or composite) have been explored widely (especially in LSBs), as carbon

is a versatile source for various electrochemical applications due to several advantages, such as ease of structure tenability and surface area modification.^[33–39] However, exploiting this material is underway in other AMSB chemistry as an interlayer. Therefore, this review summarizes an interlayer's critical evaluation, a promising approach to solving the notorious issue of AMSBs. To indulge in the importance of utilizing interlayer and carbon-based interlayer, we presented the brief reaction mechanisms of AMSBs, their features, key challenges, and strategies for cathode preparation (as this also requires great attention to improve the active material's utilization and capacity of the battery chemistry), which are explained briefly. Further, a detailed summary of the interlayer's need, various types, their mechanism of interaction with soluble polysulfides, and various approaches to preparing the interlayer is presented. At the end of the article, a detailed perspective of using an interlayer in the real-time application of AMSBs is presented.

2. Reaction Mechanism, Features, and Key Challenges of AMSBs

2.1. Reaction Mechanism

During discharge, the metal releases metal ions and electrons. The electrons travel through an external circuit, while the metal ions move through the electrolyte, both ultimately reaching the



Vikram Kishore Bharti is a Faraday Institute Research Fellow at the University of Southampton, working on next-generation high-performance MSBs. He holds a Ph.D. and an M.Tech in Chemical Engineering from IIT Hyderabad, with his doctoral research focusing on bacterial cellulose-derived carbon nanofibers for MSBs. His expertise includes energy storage devices, nanomaterials, bacterial cellulose, and electrochemistry. Before joining Southampton, he served as a Postdoctoral Researcher at IIT Hyderabad. Dr. Bharti aims to advance sustainable and efficient energy storage technologies through innovative material design.



Ashish Priyam Goswami is a Joint Ph.D. candidate at Monash University, Australia, and IIT Bombay, specializing in the study of Heusler compounds for thermoelectric applications. His research integrates first-principles calculations and machine learning to identify materials with optimal electronic and thermal transport properties. He holds a B.Tech in Mechanical Engineering from Tezpur University and an M.Tech in Polymer and Biosystem Engineering from IIT Hyderabad. Ashish has worked on a wide range of topics, including batteries, biopolymers, and solar energy, and has served as a Project Scientist at IIT Madras, focusing on 2D materials like MXenes and MBenes.



Mudrika Khandelwal is an Associate Professor in the Department of Materials Science and Metallurgical Engineering at IIT Hyderabad. She earned her Ph.D. from the University of Cambridge, UK, and holds B.Tech and M.Tech degrees from IIT Bombay. Her research is inspired by nature, focusing on biopolymers and composites for applications in energy, biomedical materials, and sustainable packaging. Her current work includes the development of conducting paper and antifouling materials. With expertise in cellulose composites, drug delivery, and nanotechnology, Dr. Khandelwal leads innovative research aimed at solving real-world challenges through sustainable material design.



Chandra Shekhar Sharma is a Professor in the Department of Chemical Engineering at IIT Hyderabad. He earned his Ph.D. from IIT Kanpur in 2010 and specializes in polymer and carbon nanomaterials, Carbon-MEMS, electrospun nanofibers, and nature-inspired functional surfaces. His interdisciplinary research encompasses biomedical materials, sensors, energy, and waste management. Dr. Sharma has published over 150 peer-reviewed articles, holds multiple patents, and has received several national and international awards. He has developed impactful innovations, such as carbon materials derived from candle soot and jamun seeds, as well as sanitary napkins made from nanofibers. Additionally, he cofounded Restyro Technologies to commercialize lab-developed solutions.

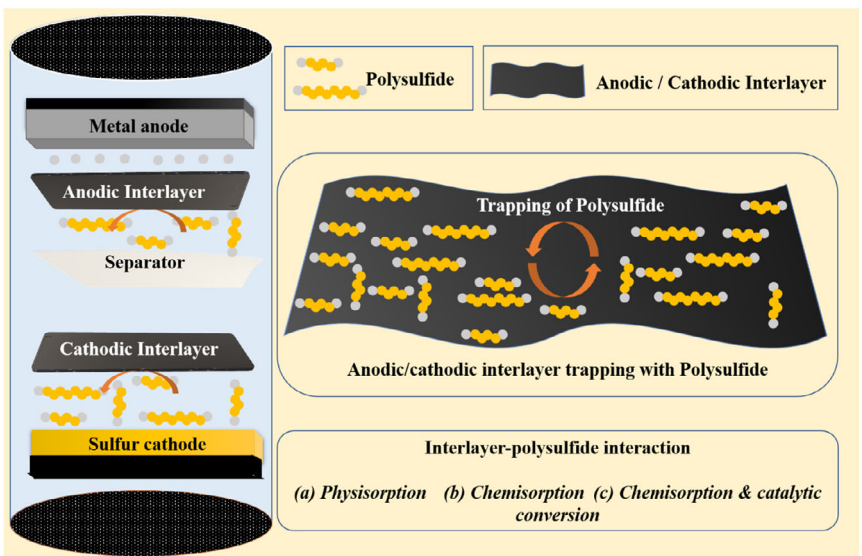
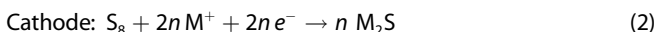
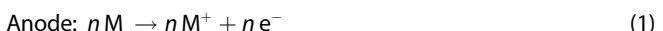


Figure 1. The schematic illustration of interlayer and soluble polysulfide interaction in AMSBs.

sulfur cathode. At the cathode, sulfur undergoes reduction, resulting in the formation of metal sulfide (M_2S) as the final electrochemical discharge product.^[40,41] For an AMSB, the electrochemical discharge reaction with the transfer of several (n) electrons is generally expressed as



However, the sulfur reduction to M_2S is not completed in one step. Initially, the long-chain polysulfides (M_2S_x , $4 \leq x \leq 8$) are formed at a higher operational voltage, which are subsequently reduced to the short-chain polysulfides (M_2S_y , $1 \leq y \leq 3$) at a lower operational voltage.^[42,43] M_2S_x is in the liquid phase, and thus its reduction to the M_2S_y (which is in the solid phase) requires a large overpotential. This overpotential varies in the order of LSB < NaSB < potassium–sulfur batteries (KSB). The largest overpotential in the case of KSB stands for another challenge: the bulky size of the K^+ compared to Na^+ and Li^+ .^[44] However, the formation of M_2S is required for the high-capacity device. The schematic for the working principle of AMSBs is shown in Figure 2.

Adopting a different active sulfur source can slightly alter the reaction pathway. The initial phases of sulfur (in general) are 1) octa-sulfur “ S_8 ” (prepared using traditional melt-diffusion strategy), 2) short-chain sulfur “ S_2 – S_6 ” (prepared by heating sulfur near its boiling point), and 3) catholyte “ M_2S_6 ” (prepared by dissolving M_2S and S_8 in the electrolyte solvent). Utilizing octa-sulfur leads to a similar reaction mechanism, as Equation (1) and (2) illustrate. In the case of short-chain sulfur, the formation of long-chain polysulfide (M_2S_8 – M_2S_6) can surpass leading to the formation of the next long-chain polysulfide, depending on the initial chain length of polysulfide used as active material (for instance, M_2S_4 when S_8 is used as an active material), and form the end discharge product (M_2S). However, the usage of catholyte follows a similar pathway

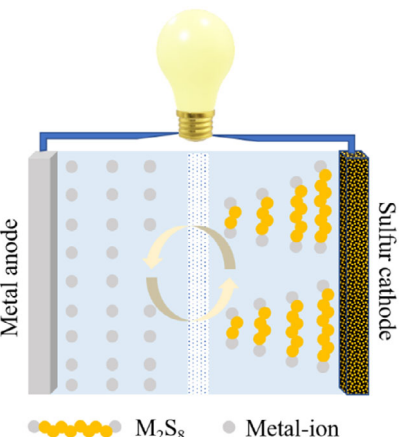


Figure 2. Schematic for the working mechanism of AMSBs.

as octa-sulfur, starting from the reduction of M_2S_x to the next shorter-chain polysulfide (for instance, M_2S_4 is formed when M_2S_6 is used as an active sulfur source). The nature of charge-discharge profiles is different in each AMSB. For example, LSB shows the capacity contribution from the plateau and the sloping region with the lowest hysteresis. However, NaSB and KSB deliver capacity in the sloping region. The sloping region can be associated with the larger ionic sizes of Na^+ and K^+ compared to Li^+ and thus higher overpotential. Table 1 illustrates the fundamental properties (such as Gibbs' free energy, cell potential, energy density, and volume variation) and reaction pathways of AMSBs.^[45]

The features and key challenges associated with the AMSBs are discussed in the following sections.

2.2. Advantageous Features of AMSBs

AMSBs have attained enormous attention due to their several advantages over LIBs. The features and challenges are discussed

Table 1. Comparing the electrochemical features of AMSBs.

AMSB chemistry ^{a)}	LSB	NaSB	KSB
Overall reversible reaction	$2\text{Li} + 1/\text{S}_8 \rightarrow \text{Li}_2\text{S}$	$2\text{Na} + 1/\text{S}_8 \rightarrow \text{Na}_2\text{S}$	$2\text{K} + 1/\text{S}_8 \rightarrow \text{K}_2\text{S}$
Gibbs' free energy for the final product [kJ mol ⁻¹]	-432.57	-357.77	-362.73
Cell theoretical voltage [V]	2.24	1.85	1.88
Gravimetric energy density [Wh kg ⁻¹]	2600	1274	914
Volume variation during electrochemical reaction [%]	80	171	308

^{a)}Values obtained from the previous report.^[41,192]

in the following section. First, sulfur has a very high theoretical specific capacity of 1675 mA h g⁻¹, which is the highest among solid-state cathode materials for rechargeable lithium batteries and surpasses that of current LIB cathodes.^[46] Therefore, sulfur as a cathode is the key to improving high-capacity AMSBs.

AMSBs bear a high energy density compared to traditional LIBs. The main difference in energy density is related to the charge-storage mechanism. LIBs work on the intercalation/de-intercalation mechanism, and thus, the energy density of the system is limited to 200–250 Wh kg⁻¹.^[47,48] However, the AMSBs work on the redox mechanism with a two-electron transfer. The sulfur-based cathode receives two electrons from the alkali metal anode and undergoes a two-step reduction. Due to this two-electron transfer and redox reaction mechanism, the energy density of the practical AMSBs is relatively higher than the traditional LIBs.^[49,50] The typical LSB can store an energy density of 2600 Wh kg⁻¹. Simultaneously, KSB can store up to 914 Wh kg⁻¹, and NaSB can store 1274 Wh kg⁻¹. The practically achievable energy density of LSBs is still 2–3 times more than that of the LIB reported by the commercial manufacturer.

Sulfur has more than 30 allotropes, with orthorhombic sulfur being the most stable form at normal temperature and pressure. It is also commonly produced as a by-product of petroleum refining and is the 16th most abundant element globally.^[51,52] Therefore, the cathodic material's cost is lower than that of traditional LIBs, where heavy metals such as Ni, Co, Mn, and Fe are used as cathode. Apart from this, the anode (potassium and sodium) has a great reserve compared to lithium (nonetheless, lithium chemistry is well-matured); thus, the anode's cost can also be reduced. Therefore, the cost of AMSBs is expected to decrease as per the currently dominant LIBs.

2.3. Major Challenges of AMSBs

AMSBs face many challenges, and this section will discuss significant challenges confronting AMSBs (Figure 3). First, sulfur and M₂S are insulating in nature, thus hampering the electronic pathway during the electrochemical reaction. This induces several issues, such as underutilization of active sulfur, poor cyclability, increased resistance, and deposition of insulating M₂S on the

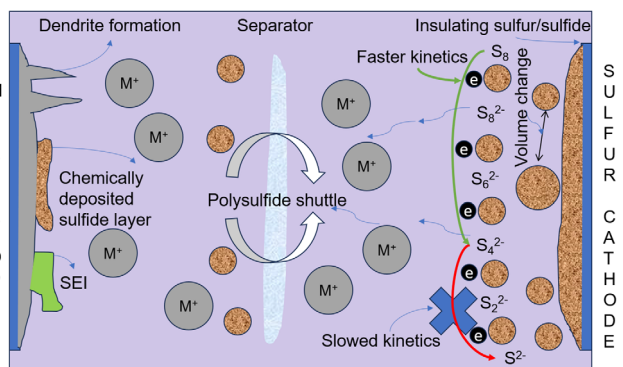


Figure 3. Schematic illustrating the key challenges of AMSBs.

electrode.^[53] In addition, the deposition of M₂S is irreversible and causes underlying electrode passivation. For making sulfur cathodes, researchers used to create intimate contact with a porous conductive host, often carbon or conducting polymer, to increase the electronic and ionic conductivity of the electrode.^[54] For instance, different carbon nanostructures, including carbon nanospheres,^[55,56] carbon nanotubes,^[57,58] carbon nanofibers,^[59] carbon aerogels,^[60] and biomass-derived carbon,^[61,62] have been reported to support the insulating sulfur in the AMSBs. Meanwhile, various conducting polymers, such as polypyrrole,^[63] polyaniline,^[64] and polyethylene dioxothiophene,^[65] have been explored.^[66]

Secondly, the intermediate polysulfides (M₂S_x, 4 ≤ x ≤ 8) are soluble in the most commonly used organic electrolytes for AMSBs. They dissolve in the electrolyte and can migrate to the anode side under the concentration gradient as a driving force. Once they are diffused to the anode side, they can reduce chemically (instead of electrochemically) and deposit on the anode, causing anode corrosion, loss of active material, and electrode passivation.^[67–71] The soluble polysulfide can also diffuse back to the sulfur cathode for reoxidation. This phenomenon is termed the "shuttle effect of soluble polysulfides." This can be understood as an internal short circuit, leading to high self-discharge and low Coulombic efficiency during charge/discharge operation.^[20] Various strategies have been developed to tackle the shuttle effect on LSBs. One common method involves using porous carbon materials to physically confine lithium polysulfides, using a free-standing cathode, while another relies on polar substances like metal oxides to chemically anchor them.^[69,72–74] Catalytic materials help speed up polysulfide conversion, reducing their accumulation.^[69,75,76] Meanwhile, changes to the electrolyte composition can lower polysulfide solubility.^[69,77,78] Modifying separators or introducing interlayers adds barriers to block polysulfide movement, and specially designed host structures combine these approaches for improved efficiency.^[28,69,79–83]

The third formidable challenge of AMSBs is the dendrite formation. The metal dendrite formed by the nonuniform deposition of metal ions is also a major problem that may cause a short circuit during cycling. The uncontrollable dendrite formation imposes remarkable safety concerns for AMSBs. Internal short circuits may happen due to the piercing made by the metal dendrite. Low Coulombic efficiency and poor cycling performance

occur due to the formation of “dead metal” in the detached dendrites.^[84,85] In the case of Na-S, Na is more active than Li and may even react with the aprotic solvents. This leads to much more severe dendrite formation on the Na surface than on the Li surface.^[86] In the case of K-S batteries, the uneven plating and stripping of potassium would lead to the growth of potassium dendrites, which might penetrate the separator and lead to internal short circuits, inducing severe safety concerns. To address the problem with the dendrite growth, the side of the separator facing the anode is often coated with either strong materials like ceramic nanomaterials that physically block dendrites from breaking through or functional additives that help control how lithium ions are deposited. These functional layers present in the Janus separator, with two distinct functional layers on two sides of the separator, the anode side functional layers restrict the puncture, help in ion transport as well as localizing the anions.^[87]

Fourth, the discharge end product and sulfur have different densities, leading to volume changes during the electrochemical reaction. These volume changes in the electrodes, which involve expansion and contraction, are seen as inevitable in batteries and can pose safety risks.^[88] Low cycle life, electrode detachment, leakage, and breakdown of electrochemical cells may happen due to the large volumetric expansion of sulfur upon the conversion reaction.^[89] A common strategy to manage volume changes in LSBs is designing porous or flexible host materials for the sulfur cathode. These include porous carbon frameworks, elastic binder-free structures, composite architectures, and functional coatings—all of which help absorb expansion, maintain structural integrity, and ensure efficient charge transport.^[90]

By doing the asymmetric modification in the sandwiched separator configuration, we can simultaneously reduce the polysulfide shuttle effect and the dendrite formation. To date, altering the surface of commercial separators or adding an interlayer is an effective and adaptable method for reducing the shuttle effect of polysulfides and preventing the growth of dendrites.^[87,91]

Another unavoidable challenge with the AMSBs is that the alkali metals are highly reactive with the electrolyte solvents. The electrolyte decomposes into a solid phase when encountering the alkali metal anode. However, the shuttle effect of soluble polysulfides makes this more complicated, and thus, on extended cycling, the interphase is not stable. This causes uneven plating/stripping of the metal anode, consumption of fresh metal in consecutive cycles, and unwanted side reactions, and thus leads to more metal consumption than required.^[42]

3. Materials of Choice for MSBs

3.1. Cathode

Sulfur is insulating; therefore, it should be added to the conducting agent, such as carbon and conducting polymers, to enable them to participate in the redox reaction. The composites are prepared with various strategies for adding sulfur to the conducting agent (**Figure 4**): 1) melt-diffusion strategy, 2) short-chain sulfur (S_4-S_6) molecule, and 3) M_2S_6 catholyte.



Figure 4. Schematic illustration of active sulfur utilization in a different form in the cathode.

3.1.1. Melt-Diffusion Strategy

The physical encapsulation of sulfur is usually performed by heating the mixture (sulfur + conducting agent) near the melting temperature of sulfur and is thus named “melt-diffusion.” In brief, the mixture is heated at $\approx 155\text{--}160\ ^\circ\text{C}$ with a dwelling for 10–15 h to enable sulfur encapsulation.^[49,92] The temperature of 155–160 °C is chosen since sulfur reaches its minimum viscosity at this temperature, and thus diffusion/encapsulation in the pores of the conducting agent can be achieved. Further, the sulfur is converted to cyclic sulfur (S_8) from its orthorhombic phase by treating it at this temperature. Moreover, the prepared composites have higher sulfur loading, as there is not much loss of sulfur at its boiling temperature. Many research articles have followed this strategy to encapsulate sulfur in the conducting agents. Following this strategy, the sulfur is physically encapsulated in the agent without any chemical interaction, and thus, in this case, the solvation of intermediate polysulfide is easier. Therefore, the cathode prepared with this strategy is severely affected by the infamous shuttle behavior of polysulfides.

3.1.2. Short-Chain Sulfur ($S_4\text{--}S_6$) Molecules

The other way of utilizing the active sulfur is to encapsulate it with the conducting agents at higher temperatures. The high-temperature treatment enables the sulfur chain (S_8) to break into fragments and thus can be attached chemically to the conducting agents. The mixture of conducting agent and sulfur is heated to the boiling temperature ($\approx 450\ ^\circ\text{C}$) of sulfur. The sulfur chains start opening when the temperature reaches $>160\ ^\circ\text{C}$, forming sulfur diradical (S_8 , liquid state). The sulfur diradical can easily break into small fragments once the temperature reaches the boiling temperature of sulfur. The mixture should be held for at least 10 h at this temperature to form the short-chain sulfur molecules. The short-chain sulfur molecules are very reactive and, thus, form a covalent bond with the conducting agent.^[93,94] This experimental method leads to the formation of covalent confined sulfur molecules, and thus, the shuttle behavior is relieved to a more considerable extent compared to the melt-diffusion approach. However, the sulfur loading decreases drastically due to high-temperature processing. A series of reports are available following this strategy. This approach is adopted chiefly for very sensitive anodes such as potassium. This is due to the highly reactive nature of the potassium anode.

3.1.3. M_2S_6 Catholyte

Using active sulfur as a catholyte has several advantages over the other two broadly explored strategies. The usage of catholyte (M_2S_6 , M = Li, K, Na) leads to an even distribution of the active material over the entire cathode surface, and thus, the utilization rate of sulfur is higher. Due to its liquid state, the catholyte enables higher loading from per commercial perspective without affecting the cathode thickness.^[60,95,96] Moreover, flexible and free-standing conducting matrices can be easily fabricated following this strategy. However, the issue with this approach is that it can react with the anode directly and can corrode it. Therefore, special attention should be paid to anode protection in this case. Compared to the previous two strategies, this approach is only explored a little in present literature.

3.2. Anode

An anode is the source of electrons and ions in the MSBs and plays a pivotal role in the electrochemical redox reaction. Alkali metals are used directly as an anode. Alkali metals have the lowest reduction potential in the electrochemical series, concerning standard hydrogen electrodes. Li has an ultralow redox potential with -3.04 V, while potassium has -2.93 V and sodium bears -2.84 V. Simultaneously, the specific capacity of the alkali metals is higher due to their lightweight and thus considered a potential anode for MSBs. However, the main challenge with bare metal is its instability during the electrochemical reaction. The soluble polysulfides diffuse to the anode and deposit on it. They are further reduced to insulating M_2S under an electric potential. Thus, the underlying metal cannot be accessed for a further electrochemical reaction.^[97,98] Therefore, the shuttle effect of the polysulfides should be rendered to create a stable and stable anode. Another challenge affecting an anode's stability is the unstable electrode-electrolyte interface. Due to the unstable interface, the fresh metal is consumed in several cycles, leading to non-judicial use of the metal. Therefore, the design of artificial interfaces can be beneficial in this direction. Researchers have forwarded several strategies to protect the anode.

3.3. Separator

A separator is an electrically insulating but ionically conducting component of a battery. It allows the passage of ions from the anode to the cathode to enable the electrochemical reaction by using electrolytes as charge carriers.^[51] An ideal separator is expected to be chemically stable (this does not allow any degradation due to reactivity with any chemical during the electrochemical reaction), mechanically strong (to bear the temperature rise during the electrochemical reaction and sustain the puncture due to dendrite formation), porous, and permeable to the electrolyte (to ensure the ionic conductivity and maintain the redox species in cathode/anode region).^[99,100] The separators used for AMSBs are mainly polypropylene, polyethylene, or sandwiched (PP/PE). However, owing to the large pore size of these separators, they are inefficient in blocking the diffusion of soluble

polysulfides due to their larger pore size. Thus, as mentioned in the previous section, they react to the anode, causing severe issues. In the literature, the researchers have also used coated separators to inhibit polysulfide diffusion and improve the electrochemical performance of AMSBs.^[101]

3.4. Electrolyte

The electrolyte is an essential part of an electrochemical device to maintain charge neutrality during the progress of the electrochemical reaction. The electrolyte is comprised of salt and solvent. Salt possesses the charges to maintain charge neutrality, and solvent imparts ionic mobility to the ion. Another essential function of the electrolyte is to transport liberated metal ions from the anode to the cathode, facilitating the redox reaction. In general, a combination of solvents (in the form of binary solvents) is used in AMSBs. The use of excess electrolytes may lead to unsafe devices severely affected by the shuttle effect of intermediate polysulfides.^[102] Therefore, the devices based on AMSBs can operate at a lower electrolyte dosage. This lower electrolyte dosage is taken very seriously in LSBs, and various reports are available where the lean electrolyte is explored. The next section elaborates on the design of an interlayer, their need, the classification of various types based on interaction with the soluble polysulfides, and their position in the battery assembly.

4. Designing an Interlayer: A Protective Layer for Safe and Long-Life AMSBs

4.1. Need for a Protective Interlayer

An interlayer acts as a protective barrier that helps minimize the loss of active material during electrochemical reactions by mitigating the shuttle effect of soluble polysulfides. This shuttle effect is a major challenge in metal-sulfur batteries, as discussed in Section 2.3. Solvent molecules solvate long-chain intermediate polysulfides, which then diffuse to the anode side due to a concentration gradient, leading to harmful consequences. To address this, researchers have focused on trapping these soluble polysulfides within the cathode region to prevent them from reacting with the anode, thereby preserving the active material. An interlayer plays a key role in preventing the diffusion of polysulfides to the anode. Positioned between the cathode and separator or the anode and separator, the interlayer captures the soluble polysulfides. These trapped polysulfides can be reused in subsequent cycles, improving sulfur utilization.^[25,103] The interlayer can be classified into various types, summarized in the next section.

4.2. Classification of Interlayers

Based on the physical state of an interlayer, they can be broadly classified into two subcategories: 1) modified separator interlayer^[104] and 2) free-standing interlayer^[39,105] (Figure 5a,b). The separator in the former example is covered with materials that have an affinity for soluble polysulfides. This separator absorbs

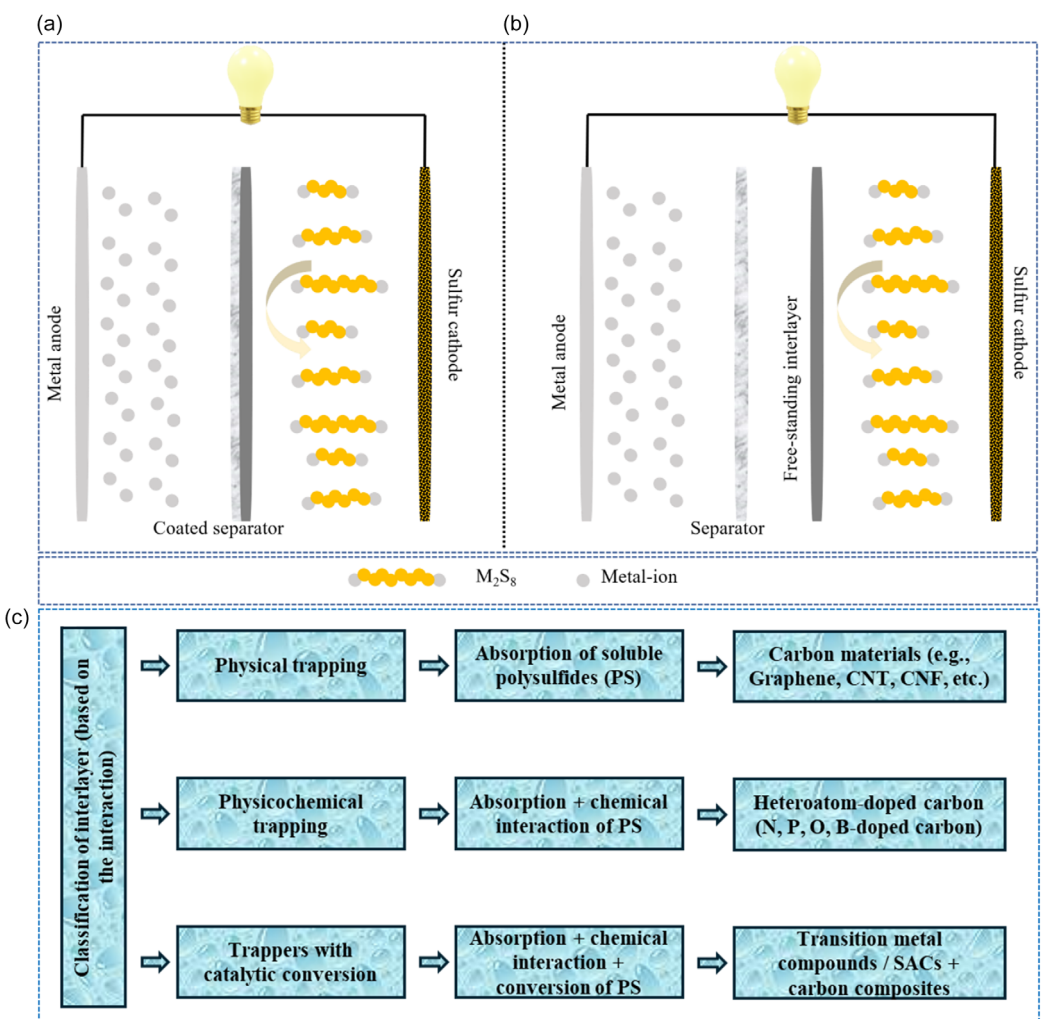


Figure 5. Schematic for the type of interlayers based on their physical state: a) coated separator, b) free-standing interlayers for AMSBs, and c) classification of interlayers based on the interaction with polysulfides.

the soluble polysulfides and stores them within the cathode region for use in subsequent cycles. However, the free-standing film is inserted between the cathode and separator in the latter situation. The film can be coated with an active material (which has an affinity to interact with soluble polysulfides), or a bare carbon film can be used. In the latter case, the free-standing film must be carbonized so as not to affect the electronic conductivity and thus is also called an upper current collector. In the separator modification case, the separator should not be conductive to prevent a short-circuit, and the coated side is kept facing toward the anode or cathode.

Further, the interlayers can be classified based on their interaction with the soluble polysulfides: 1) physical trappers, 2) physicochemical trappers, and 3) trapping with catalytic conversion (Figure 5c). The physical trapper-type interlayer absorbs the soluble polysulfides on its surface/bulk without any chemical or electrostatic interactions.^[106] The specific surface area of the interlayer is vital in this case, as the higher the surface area the higher the storage capability. Therefore, a porous substrate with a higher specific surface area is an ideal choice for this type of interlayer. Carbon materials are best suited for the physical trapper type

interlayer category as they can easily be tuned for the porous and high specific surface area as per requirement. However, this type of interlayer can only be effective for a short time and shorter cycle life, as the surface will get saturated with absorbed polysulfides. Therefore, the physical and chemical trappers are getting intense consideration due to their dual role in trapping soluble polysulfides. First, physical trapping enables the storage capability of the polysulfides in their porous structure. Second, they can chemically or electrostatically interact with the polysulfides, thus minimizing their diffusion. The strong interaction can hold the polysulfides for extended periods, avoiding the problem associated with the physical trapper. For this purpose, heteroatom-doped carbon can be a better choice as the presence of heteroatoms can change the molecule's polarity, and thus they can easily bind with the polysulfides. These heteroatoms include nitrogen, boron, oxygen, sulfur, and phosphorus doping.^[107,108] Even the physical and chemical trappers have limitations due to limited adsorption sites for the soluble polysulfides. Therefore, researchers moved to a new class of trapping strategies termed trappers with catalytic conversion. In this class of interlayers, the interlayer comprises electrocatalytic species that

can convert the soluble polysulfides to the desired end product. Transition metal compounds (oxides, nitrides, sulfides, tellurides, selenides, and phosphides) and single-atom catalysts (SACs) have emerged mainly for this purpose.^[26,38,109,110] Among these class materials, the selected species, such as Fe, Co, Mo, and Ni-based compounds, act as catalysts for soluble polysulfides and convert them by forming an intermediate complex (thiosulfate).^[111] This thiosulfate then captures the further coming polysulfides, forms polythionate, and releases the end discharge product as a reaction by-product. The key aspects for these materials to obtain an effective conversion and capture ability are 1) electronic conductivity, 2) catalytic activity, and 3) specific surface area.

Among the transition metal compounds, sulfides have higher catalytic activity owing to the easy insertion of an S–S bond to generate a polythionate complex, which acts as a binding site for consecutive long-chain polysulfide species. However, the specific surface area and electronic conductivity are compromised. On the other hand, transition metal nitrides have better electronic conductivity, while the catalytic activity is lower than the sulfides, and the specific surface area is between the oxides and sulfides. Meanwhile, the oxides have better catalytic activity compared to the nitrides and lower than the sulfides; however, the specific surface area is the highest among the transition metal compounds.^[112–114] On the other hand, SACs have emerged to have outstanding catalytic activity owing to the localized tuning and special confinement.^[115] However, the connectivity is quite poor between different SAC molecules, and the low specific surface area for polysulfide absorption.^[116] To tackle the aforementioned challenges with transition metal compounds and SACs, it is essential to add carbon support to achieve the desired level of polysulfide absorption and conversion to enable the long cycle life of MSBs. Introducing carbon support increases the specific surface area and electronic conductivity to the desired level;

thus, absorption of polysulfides can be boosted.^[117] The mechanism and literature in this direction are presented in the following sections.

The interlayer can further be classified based on its position in the assembly of AMSBs as 1) anodic interlayer and 2) cathodic interlayer (Figure 6). An anodic interlayer is inserted between the anode and separator, while a cathodic interlayer is inserted between the cathode and separator. These interlayers serve as a reservoir for storing the soluble polysulfide and an upper current collector. Anodic interlayers have an additional advantage as they can enable even plating/stripping of the metal ion during the cell operation. Therefore, the dendrite formation at the metal surface may also be reduced substantially. The following section summarizes the different carbon-based materials used as an interlayer.

4.3. Synthesis/Fabrication Methods for Interlayers

Interlayers are a vital component in AMSBs, playing a key role in improving their overall performance, positioned between the cathode and separator, or between the separator and the anode. Like separators, interlayer materials must meet several strict requirements to function effectively. They should be porous with good electrolyte wettability, mechanically flexible and elastic, and must allow rapid diffusion of metal ions (M^{+}), while remaining electronically insulating to prevent internal shorting.^[118,119] Just as with cathodes and separators, interlayers are also expected to suppress polysulfide migration to enhance cycling stability.^[118,119] To meet these demands, various strategies and material designs have been developed, leading to significant progress in the synthesis and engineering of high-performance interlayers for AMSBs. As already mentioned, the interlayers can be broadly classified into two categories: free-standing interlayers and coated separators, as discussed below.

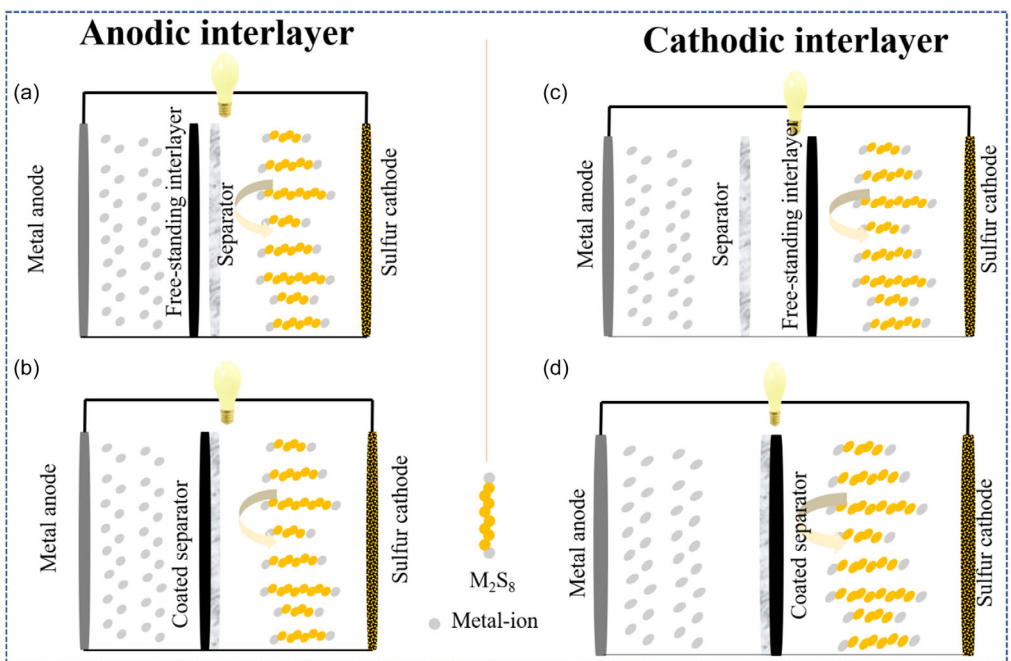


Figure 6. Schematic illustration of a,b) anodic interlayer and c,d) cathodic interlayer.

The fabrication of freestanding interlayers for AMSBs generally involves two main steps: first, forming a compact and independent layer, and second, punching it into small discs using a tablet punching machine.^[118] The method used to create the initial layer depends on the starting material, which can either be a powder or an existing film.^[118] These can be synthesized following a powder-based approach, including techniques such as electrospinning,^[120–122] wet spinning,^[123] slurry casting,^[124–126] vacuum filtration,^[127,128] soaking and drying^[129,130] and self-assembly.^[131–133] These methods shape loose powders into cohesive, porous structures. In contrast, film-based interlayers are commonly produced through advanced techniques like high-temperature carbonization,^[39,134–136] chemical vapor deposition,^[137–139] or atomic layer deposition,^[140,141] which offer precise control over thickness and uniformity. Once fabricated, interlayers can be directly inserted between the cathode and separator, especially when using materials like freestanding porous multiwalled carbon nanotube paper,^[28] carbon cloth,^[142] or carbonized cotton cloth.^[39] These structures can serve as upper current collectors and simultaneously act as physical barriers against polysulfide migration, enhancing the cycling stability of AMSBs.

In other instances, such interlayer substrates require further functionalization to improve their ability to trap sulfur species or facilitate the reversible conversion between various polysulfide intermediates and elemental sulfur. These enhancements are typically achieved through physical treatments, atomic doping, the introduction of chemical compounds, or combinations of these methods.^[137,143–145] Each of the methods aimed at strengthening the interlayer's physical confinement and chemical reactivity to boost battery performance.

Another effective and widely adopted method for creating interlayers in AMSBs is by coating the separator. A common example involves applying a layer of conductive carbon, such as commercial carbon black, onto one or both sides of the separator.^[146] This is typically achieved using a tape-casting technique,^[147,148] where a pre-prepared carbon slurry is evenly brushed onto the separator surface and then dried by heating in an oven for several hours.

Free-standing interlayers are generally considered more effective and reliable than the coated separator, as they often face issues such as uneven surface coverage, which can hinder performance consistency and complicate large-scale standardization.^[118] Moreover, their weak adhesion to the underlying substrate may lead to structural instability during battery discharge, negatively impacting long-term cycling performance.^[118]

4.4. Bare Carbon Interlayers

This interlayer class works on the soluble polysulfide's physical adsorption over the interlayer's available surface area. Carbon materials are best suited in this class of interlayers (such as graphene, carbon nanotubes (CNTs), and carbon nanofibers (CNFs)). To minimize the shuttle effect by blocking the polysulfide, an interlayer is introduced between the cathode and separator while cycling the cell, which will also act as an upper current collector. The carbon-based interlayers are getting enormous attention due

to their ability to block higher-order polysulfide dissolution into the electrolyte. For instance, Bharti et al.^[149] explored the same precursor as an interlayer and an interlayer for a decreased interfacial property. The candle soot (collected from the tip of the burning candle to avoid wax content) and sulfur composite were used as a cathode. In contrast, the same carbon (candle soot) was drop-cast over the electrode to enhance the electrochemical performance. The study reveals that for LSB, even at a high current rate, this interlayer effectively absorbs long-chain lithium polysulfides. The rate capability test (Figure 7a) showed that the candle soot inbuilt interlayer is effective in blocking polysulfides and preventing their dissolution into the electrolyte. Additionally, a long cycling stability test was performed to elucidate the role of the interlayer during the extended cycle (Figure 7b). The integrated candle-soot carbon interlayer significantly enhances electrochemical performance. The shuttle factor was calculated using the Newton-Raphson method to comment on the reduction of the polysulfide shuttle effect. Figure 7c depicts the plot of the shuttle factor versus the cycle number, illustrating the cyclic stability, while Figure 7d depicts the shuttle factor at various current rates, illustrating the rate performance. The variation implies the reduction in the polysulfide shuttle effect when the interlayer was cast over the electrode. In another continued study, Bharti et al.^[150] showed the feasibility of using combustion by-product candle soot as an interlayer over the electrode prepared by the solvent evaporation method on sulfur-incorporated carbonized coconut husk-sulfur composite cathode. Coconut husk was used due to inherent minerals that could help in trapping polysulfide, while the candle soot overlayer was further introduced to have a reservoir over the cathode itself. The stability test of the interlayer modified cell not only delivered a capacity of 500 mAh g⁻¹ after 100 cycles showing the capacity of the battery for long cycling but also maintained the Coulombic efficiency of 98.4% along with capacity retention of 98% (Figure 7e), which emphasize the role of candle soot over layer in blocking the polysulfides, thereby minimizing the active material loss.

Further in this direction, Huang et al.^[151] fabricated a free-standing Fe₃C/carbon nanofiber (CNF) film as an interlayer for LSBs following a one-pot electrospinning method (Figure 8a). A comparative study with and without interlayer-modified cells was performed to substantiate the role of the as-synthesized interlayer. The cell with interlayer delivered a specific capacity of 1177 mAh g⁻¹ and retained 76% of its initial capacity after 100 cycles. The enhanced electrochemical performance was related to the utilization of an interlayer that decreases the shuttle effect. Later, Manoj et al.^[152] reported polyaniline-coated mesoporous carbon to modify the sulfur cathode, whereas a flexible CNT interlayer was used for LSB assembly (Figure 8b,c). Using the CNT interlayer, the battery's overall efficiency improved due to high electrical conductivity and reduced shuttle effect by localizing the migrated polysulfides within the cathode region. As a result, the cell delivered an initial discharge capacity of 1137 mAh g⁻¹ at a 0.2 C rate. During long cycling, the cell delivered a discharge capacity of 968 mAh g⁻¹ and retained 700 mAh g⁻¹ after 200 cycles, corresponding to an extremely low-capacity decay of 0.14% per cycle. Singhal et al.^[153] also demonstrated that using an interlayer made of carbonized polyacrylonitrile (PAN)

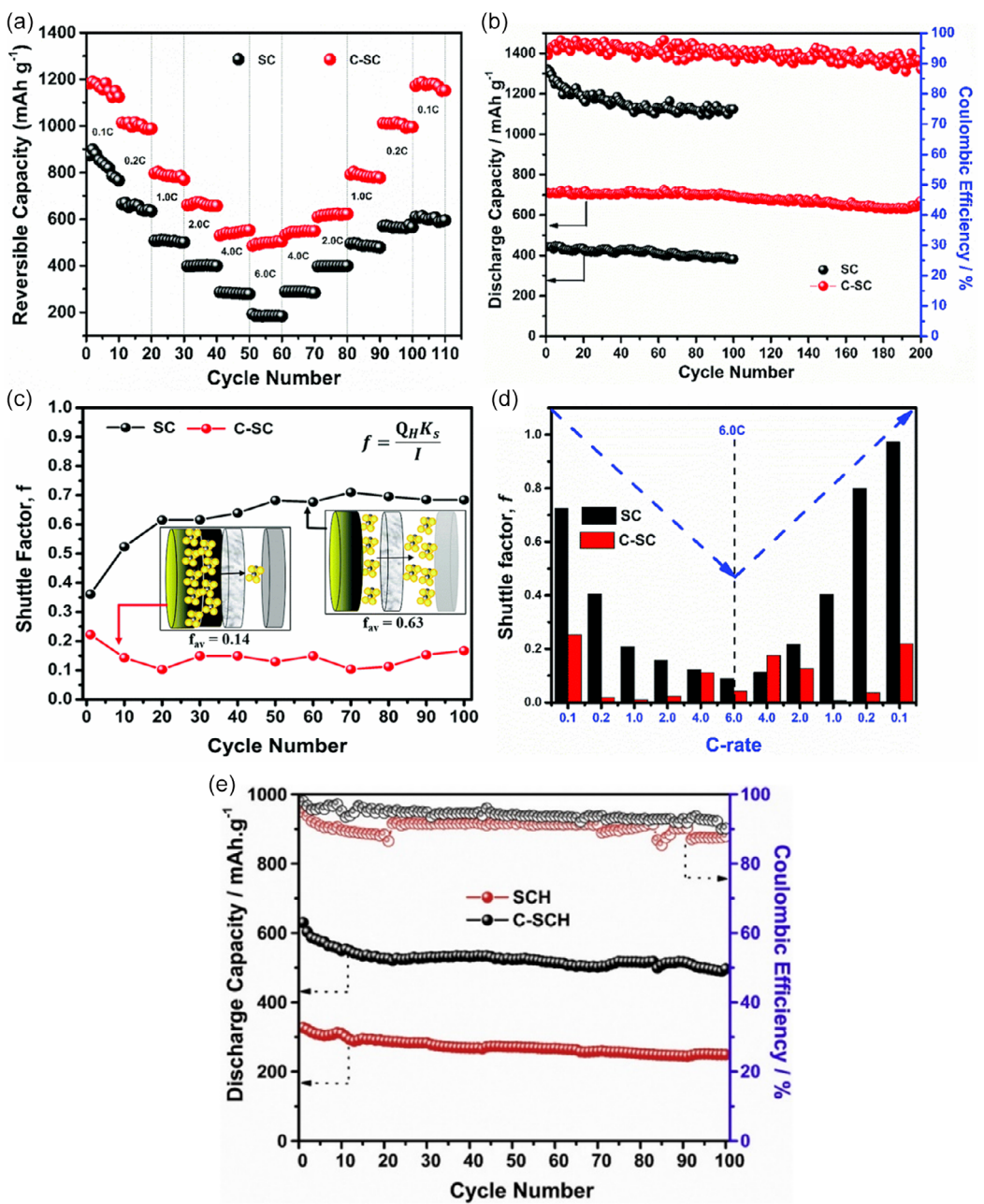


Figure 7. a) Rate performance, b) cyclic stability at 1 C, c) shuttle factor analysis during the cyclic stability tests, and d) shuttle factor analysis at various current rates for SC (without interlayer) and C-SC (with interlayer). Reproduced with permission.^[149] Copyright 2021, Royal Society of Chemistry.^[149] e) Stability profile of the cell at a current density of 1000 mA g⁻¹, illustrating the effects of the presence and absence of a carbon interlayer. Reproduced with permission.^[150] Copyright 2020, Elsevier.^[150]

nanofibers, with carefully optimized thickness, a large surface area, and a meso-microporous structure, significantly improved battery performance. Their design achieved an initial discharge capacity of 1549 mA h g⁻¹ at a C/5 rate, which corresponds to 92% of sulfur's theoretical capacity. Moreover, the system maintained an average Coulombic efficiency of 98% and retained 83% of its capacity after 100 cycles.

In another strategy, by simple treatment procedures, Kong et al.^[31] obtained a porous carbon paper from corn stalks. They used it as an interlayer for LSB to stabilize the surface morphology of the lithium anode. Yan et al.^[154] developed an

ultrathin and lightweight interlayer with MoS₂/CNT. MoS₂ nanosheets were loaded onto a cross-stacked CNT film and used as an interlayer. The interlayer-modified cell showed an initial capacity of 1237 mA h g⁻¹ and an extremely slow capacity decay rate of $\approx 0.061\%$ per cycle over 500 charge/discharge cycles at 0.2 C. Later, Cheng et al.^[155] prepared Fe₃O₄ nanoparticles/GO that act as interlayer and upper current collectors for LSBs. The rGO sheet helped in blocking the polysulfide and enabled efficient electron transport. Further, Fe₃O₄ has a great affinity toward soluble polysulfides and thus inhibits the dissolution of LiPSs significantly. Hu et al.^[156] prepared uniform SnO₂/r GO onto

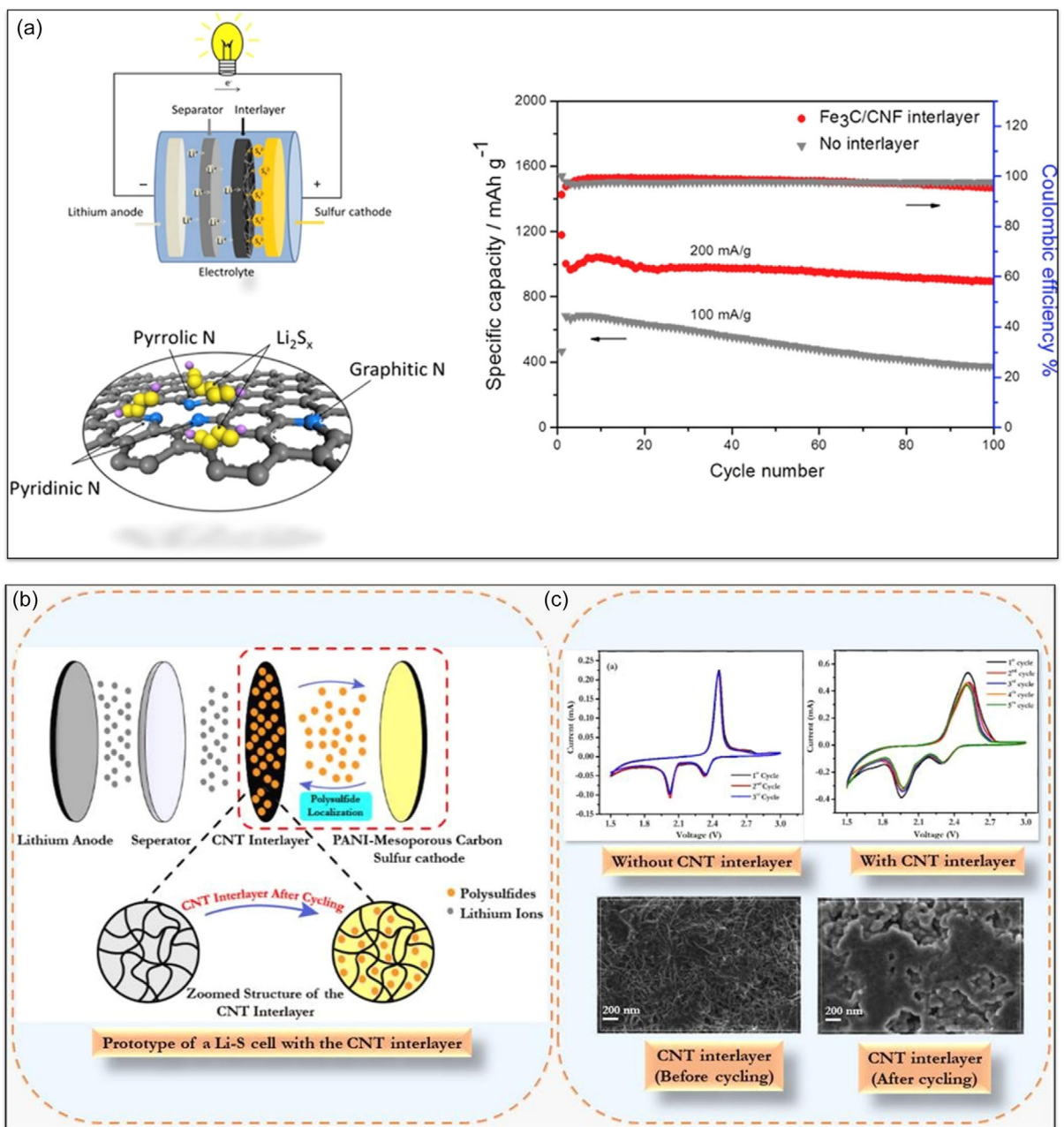


Figure 8. a) Schematic representation of LSB cell configuration with an interlayer, illustrating the trapping of polysulfides through surface interactions, and the cyclic performance of LSB. Reproduced with permission.^[151] Copyright 2015, Elsevier.^[151] b) Prototype of a typical LSB incorporating a CNT interlayer in the cathode region and c) CV curves at 0.1 mV s^{-1} and interlayer morphology before and after cycling. Reproduced with permission.^[152] Copyright 2018, Elsevier.^[152]

the polypropylene separator for use as a modified functional interlayer for LSBs. The cell showed a discharge capacity of 734 mAh g^{-1} over 200 cycles at 1C and a rate capability with an average discharge capacity of 541.9 mAh g^{-1} at 5C. The interlayer had promising anchoring capability with the S_8^{2-} cluster and LiPSs. Simultaneously, the SnO_2 also formed strong Li—O/Sn—S/O—S bonds and thus chemisorbed LiPSs that helped reduce the shuttling effect in Li—S. In yet another work, glass fiber was modified by coating to suppress the shuttle effect. Zhu et al.^[157] used different degrees of reduction to synthesize the rGO to form an interlayer for LSBs and delivered a capacity of 733 mAh g^{-1} after 100 cycles. Similarly, Luo et al.^[158] used

first-principles calculations to investigate room-temperature NaSBs and discovered that creating sulfur vacancies in MoS_2 significantly improves its ability to trap polysulfides and boosts both catalytic activity and ion/electron conductivity. Building on this, they developed a novel $\text{MoS}_{2-x}/\text{carbon}$ ($\text{MoS}_{2-x}/\text{C}$) composite, where ultrathin, flower-like MoS_{2-x} nanosheets are confined inside hollow carbon spheres using a “ship-in-a-bottle” approach. This clever structural design allows for a high sulfur loading of up to 75 wt%. As a result, the RT-Na/S batteries using this composite show excellent cycling stability with 85.2% capacity retained after 100 cycles at 0.1 A g^{-1} and outstanding rate performance, reaching 415.7 mAh g^{-1} at 2 A g^{-1} , along with a high energy density.

These strategies have also been adopted to improve the performance of NaSBs. For instance, Saroha et al.^[159] developed a cathodic interlayer using V_2O_3 nanoparticle-decorated CNF. The detailed analysis showed 70%, 54%, and 33% utilization of active sulfur with V_2O_3 nanoparticle-decorated CNF interlayer, CNF interlayer, and without an interlayer, respectively. The usage of V_2O_3 nanoparticles is promising as it increased sulfur utilization. Further, the cell delivered $\approx 100\%$ of Coulombic efficiency with 406 mAh g^{-1} at 1 C after 500 cycles. The improved electrochemical properties of as-fabricated NaSB can be ascribed to the interlayer that retains the soluble polysulfides and can be used for further cycling.

Similarly, anodic interlayers can be prepared by coating carbon materials on the anodic side of the separator or freestanding film between the anode and the separator.^[160] Following a double Fischer esterification reaction, Ye et al.^[161] prepared an interlayer by agglomerating vulcan XC72 carbon black nanoparticles into ellipsoidal superstructures, MAXC (modularly-assembled

XC72 carbon black) interlayer. The introduction of an interlayer to the cell could improve the electrochemical performance at different current densities (Figure 9a). Further, The GCD profiles have similar attributes to the LSBs, where maximum capacity was delivered by the liquid-to-solid conversion of the polysulfides (Figure 9b). Introducing the interlayer was also beneficial for improving the charge-transfer resistance compared to the cell without the interlayer (Figure 9c). The cell with this interlayer showed a Coulombic efficiency of $\approx 99\%$, maintaining for 500 cycles (Figure 9d). For the practical applicability of the interlayer, electrochemical performance was also investigated using an electrode with a sulfur loading of 5.3 mg cm^{-2} . This Li-S cell displayed excellent cyclability, delivering an aerial capacity of 4.75 mAh cm^{-2} after 100 cycles when investigated at 0.1 C (Figure 9e,f). The improved electrochemical performance was explained to be due to the introduction of a highly efficient MAXC interlayer to the LSB cell fabrication that efficiently traps the soluble polysulfides, thus reducing the infamous shuttle effect.

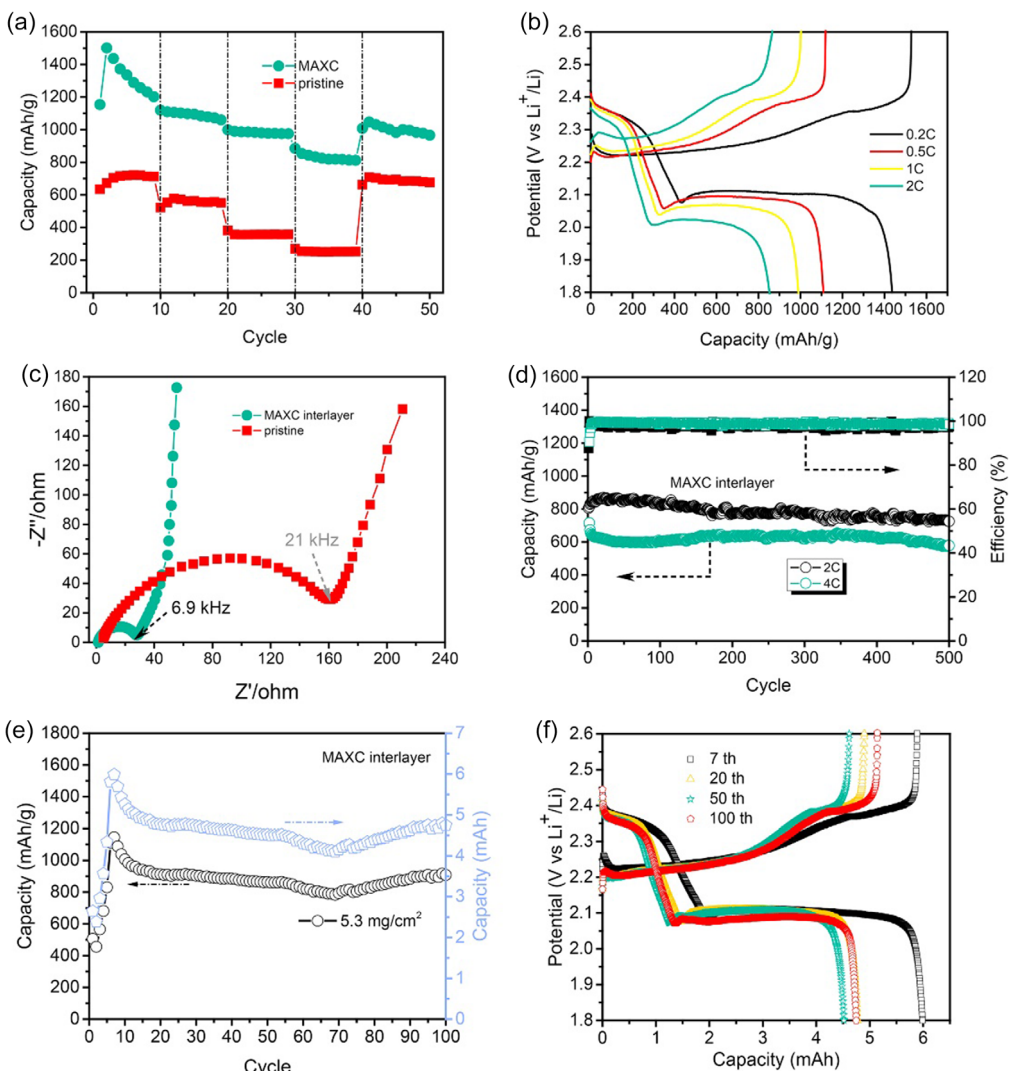


Figure 9. Electrochemical performance of the cells, including a) rate capability, b) GCD profiles at different C-rates, and c) EIS profiles of cells with and without the MAXC interlayer. Additionally, d) cyclability of cells with the MAXC interlayer at high rates, e) cyclability, and f) GCD profiles of selected cycles of LSB incorporating an MAXC interlayer with a 5.3 mg cm^{-2} sulfur loading at 0.1 C. Reproduced with permission.^[161] Copyright 2017, Elsevier.^[161]

In the report by Wu et al.^[162] a carbonized silk nanofiber film was used as a cathodic and an anodic interlayer for LSBs to reduce the lithium corrosion and shuttle effect (Figure 10). After 500 cycles, the discharge capacity was retained at 655 mAh g^{-1} at 1 C with a 97.3% Coulombic efficiency. Later, Li et al.^[163] showed that different MOF-based materials as anodic interlayers can enhance cell performance. Their detailed analysis correlated the dependence of chemical composition and particle size on the performance of LSBs.

Using an interlayer in LSBs and sodium–sulfur batteries (NaSBs) has shown drastic improvement in the electrochemical performance. Therefore, Bharti et al.^[33] explored the use of carbonized bacterial cellulose (CBC) as both a cathode host and an anode-protective interlayer in KSBs. Introducing an anodic interlayer was explained to reduce the sensitivity of the potassium anode due to the polysulfide's shuttle effect. As a result, the KSB cell with CBC interlayer could achieve stable cycling at a current rate of 2 C for up to 500 cycles, retaining a capacity of 62%. They further explored first-principles calculations to understand the efficacy of CBC's functional group presence, which benefited during the trapping of soluble polysulfide. In the following approach, Ashish et al. explored the *in situ* banana fiber-modified CBC as a cathode host while CBC as an interlayer for KSBs.^[21] *In situ* modification improved the surface area of the cathode host owing to the hierarchical structure and thus the electrochemical performance. As a result, the cell was able to deliver 473 mAh g^{-1} at 0.2 C and retained 193 mAh g^{-1} at 1.2 C. This improved electrochemical performance can be ascribed to the inclusion of banana fiber in the CBC structure, which contains inherent N-doping and thus improves the electrical conductivity properties of the cathode host. Table 2 summarizes the works performed using a carbon interlayer for LSBs.

The electrochemical performance of the AMSBs has evidenced the improvement using a carbon-based interlayer. The soluble polysulfides are physisorbed on the surface of carbon materials. However, the interaction of polysulfide with bare carbon is weak, and thus, the modification of the carbon surface can boost its adsorption capability. The following section summarizes

the approaches to modifying the carbon surfaces for enhanced surface properties.

4.5. Heteroatom-Doped Carbon Interlayers

Bare carbon interlayers have a low affinity toward soluble polysulfides. Therefore, doping with heteroatoms like N, B, O, P, and S without increasing significant weight can provide a polar structure to the carbon interlayer. This modification may create active binding/trapping sites for soluble metal polysulfides. In this direction, Kim et al.^[164] used CNTs as sulfur reservoirs and interlayers via thermal treatments under different atmospheres (oxygen and hydrogen, Figure 11a). They performed the electrochemical performance with a high sulfur loading (2.5 mg cm^{-2}) cathode coupled with an HCNT (CNT annealed with H_2 gas) or OCNT (CNT annealed with O_2 gas) interlayer and thus improved the specific capacity and cyclic performance (250 cycles). This improvement was explained as the effective blocking of polysulfides enabled by oxygen functionalization of the interlayer.

To improve the cycling lifespan by decreasing the shuttle of polysulfides and optimizing sulfur utilization, Wu et al.^[165] used a 3D N-doped graphene-coated separator as an interlayer for LSBs that delivered a reversible capacity of 852 mAh g^{-1} after 200 cycles at 0.2 C and retained 88.7% after 300 cycles at 0.5 C. The improved performance can be attributed to N-doping, which enabled polysulfide trapping, while graphene helped improve electronic conductivity for efficient electron transfer. Similarly, Wang et al.^[166] designed a freestanding uniformly distributed metallic tin-modified and N-doped carbon skeleton as the interlayer to act as an absorbent of polysulfides and a catalyst to promote the conversion of sulfur species by tin nanoparticles. The electrochemical investigation revealed enhanced performance with an initial capacity of 1123 mAh g^{-1} , retaining 92.8% after 100 cycles when tested at 0.2 C. In another report by Yang et al.^[167] sulfur-doped microporous carbon interlayer was used for LSBs with a very high specific surface area of $3211 \text{ m}^2 \text{ g}^{-1}$ that can store larger quantities of soluble polysulfides. Sulfur-doping enabled catalytic behavior in the interlayer, and as a result, the fabricated cells with this interlayer showed a low-capacity decay rate of 0.057% per cycle with a cycle life of 500 when investigated at 2 C.

Later, researchers focused on developing a codoped structure to enhance the properties of the interlayer further to ensure high conductivity and effective trapping of metal polysulfides that can be utilized during prolonged cycling. For instance, Yang et al.^[168] used a functional interlayer of tungsten oxide-decorated N, S codoped carbon nanofibers for LSBs. The cell with developed interlayer delivered an initial capacity of 1444 mAh g^{-1} and retained 1080 mAh g^{-1} after 100 cycles at 0.2 C and a superior rate capability of 946 mAh g^{-1} at 2 C. Here, N, S, and WO_3 uniform distribution over the interlayer enhanced the redox reaction kinetics by providing strong chemical anchoring sites for binding the LPSs. Similarly, Jiang et al.^[169] prepared flexible interlayers for LSBs by N, S codoped hierarchical porous biomass carbon sample with a unique honeycomb-like micro/mesoporous structure with a very high specific surface area of $2543.8 \text{ m}^2 \text{ g}^{-1}$ (Figure 11b,c).

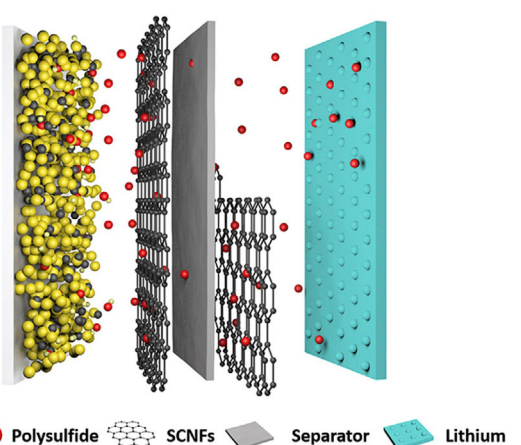


Figure 10. Schematic representation of the cell assembly using carbonized silk nanofiber. Reproduced with permission.^[162] Copyright 2019, Springer.^[162]

Table 2. Summary of carbon-based interlayers for cathode protection in LSBs.

S. N.	Cathode	Interlayer	Electrochemical performance Initial reversible capacity/No of cycles/ capacity retention ^{a)} /C rate or current density [mAh g ⁻¹ /n%/C or A g ⁻¹]	Performance enhanced after interlayer inclusion
1	S/coconut husk carbon ^[150]	Candle soot carbon	504/100/98/2.0	Capacity retention has increased by 22%
2	Bare sulfur ^[193]	rGO	1322/200/49/0.2	Thermal stability, specific capacity, cycle life, and capacity retention increase
3	Bare sulfur ^[194]	Bamboo char	813/300/74/1.0	Improved Coulombic efficiency (\approx 98%), cycle life, rate capability, and minimized capacity decay (0.11% per cycle)
4	S/CNT composite ^[195]	rGO/carbon black	1260/100/71/1.6 A g ⁻¹	Coulombic efficiency and cyclic stability are improved
5	Bare sulfur ^[167]	Luffa sponge	1000/500/80/2.0	Exhibits excellent initial reversible capacity, enhanced rate capability, and capacity decay rate also became minimum (0.057% per cycle)
6	Bare sulfur ^[157]	rGO with different reduction species	733/100/70/2.0	rGO with a higher reduction degree showed better capability in rejecting polysulfides and thus showed better electrochemical performance
7	Bare sulfur ^[39]	Waste cotton	827/1000/58/1.0	Cycling stability and rate capability have improved
8	Bare sulfur ^[156]	Uniform SnO ₂ /rGO	914/200/80/1.0	Showed high discharge capacity and rate capability
9	Bare sulfur ^[196]	Fe ₃ O ₄ /Graphene	727/2000/49/1.0	Enhancement of rate capability and cyclic performance and also exhibits an extremely low capacity decay rate (0.02% per cycle)
10	Bare sulfur ^[197]	Microporous carbon paper	1367/150/85/2.0	Improvement in active material utilization and capacity retention
11	S/coconut shell carbon ^[155]	Fe ₃ O ₄ /rGO	850/200/66/0.5 A g ⁻¹	Shows superior rate performance, high initial specific capacity, and excellent cycling stability
12	Bare sulfur ^[151]	Freestanding Fe ₃ C/CNF	1177/100/76/0.2 A g ⁻¹	Delivers an outstanding specific discharge capacity, and capacity retention
13	Bare sulfur ^[134]	Carbonized egg membrane	1327/100/75/0.1	Improves the discharge capacity and the long-term cycle stability
14	S/polyaniline coated carbon ^[152]	CNT	1137/50/69/0.2	Delivers a good initial discharge capacity, and exhibited a low capacity decay of 0.14% per cycle
15	S/bamboo carbon ^[31]	Porous carbon	—	—
16	Bare sulfur ^[154]	MoS ₂ /CNT	1237/500/94/0.2	Exhibits an improved specific capacity at a high capacity rate, long cycle life, and a low capacity fade rate (0.061% per cycle)
17	S/Super P ^[162]	Silk-derived fiber	1164/200/69/0.2	It shows better Coulombic efficiency, reversible capacity, and a low average capacity loss (0.018% per cycle).
18	Bare sulfur ^[163]	MOF (Y-FTZB)	1101/51/300/0.25	Enhances the cycling stability and initial specific capacity

^{a)}Capacity retention = (nth cycle capacity/1st cycle capacity) × 100.

Following this strategy, an initial discharge capacity of 1549 mAh g⁻¹ at 0.1 C was delivered. Further, the cell showed a reversible capacity of 609 mAh g⁻¹ after 300 cycles with a capacity decay of 0.06% per cycle at 0.5 C.

In the other work by Gu et al.^[170] thermal annealing and subsequent hydrothermal reaction routes were adopted to synthesize a conductive, porous N and P codoped graphene interlayer for LSBs. The dopant concentration of N and P was \approx 4.38% and 1.93%, respectively. The cell with this interlayer delivered an initial capacity of 1158.3 mAh g⁻¹ at 1 C with excellent cyclability (capacity fade rate of 0.09% per cycle). Further, Wang et al.^[171] worked on designing a porous-CNT/S cathode coupled with a lightweight multifunctional porous S and N codoped graphene interlayer for LSBs. Increased electronic conductivity, reduced

mitigation of LiPSs, modulated Li₂S/Li₂S₂ growth, and protected separator's integrity are the major reasons for enhancing the electrochemical properties of the battery. **Table 3** summarizes the work with heteroatom-doped carbon matrices used as an interlayer for LSBs.

4.6. Transition Metal Compounds and Carbon Composite Interlayers

Carbon and heteroatom-doped carbon can anchor the soluble polysulfides through physical or chemical absorption. However, efficient trapping is short-lasting as the available surface area/active site can be saturated after accumulating soluble polysulfides, depending on the available specific surface area for their

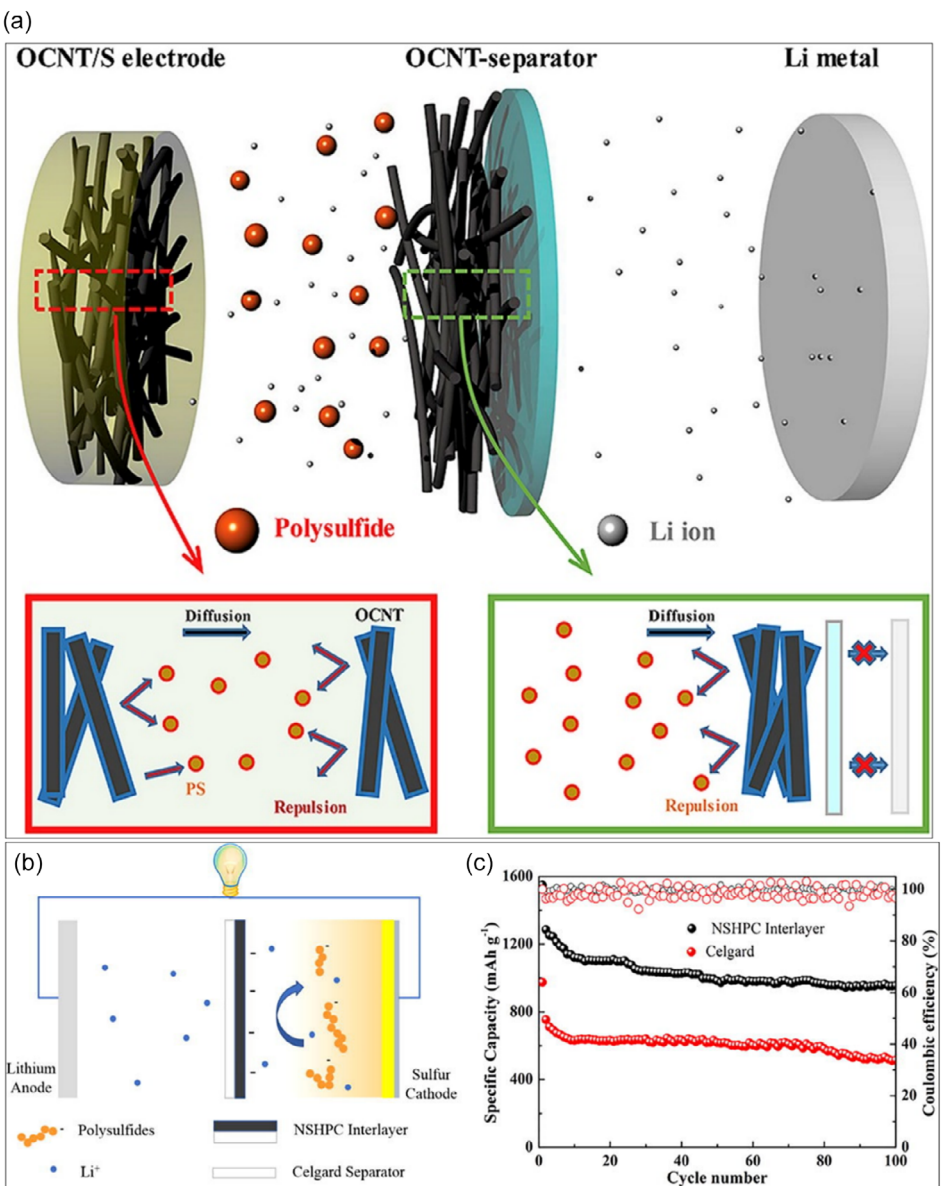


Figure 11. a) Schematic illustration demonstrates the LSB configuration and the function of OCNT as sulfur reservoirs and interlayer barriers during the discharge process. Reproduced with permission.^[164] Copyright 2018, Elsevier.^[164] b) Illustration of LSB with NSHPC interlayer and c) long-cycling at 0.1 C, with and without NSHPC flexible interlayer. Reproduced with permission.^[169] Copyright 2019, Elsevier.^[169]

absorption. Therefore, the scientific community focused on developing materials with catalytic activity toward soluble polysulfides. The material can bind the polysulfides and convert them to the end discharge product (M_2S_2 or M_2S). This class of materials is termed electrocatalysts, and in general, transition metal compounds (such as oxides, nitrides, and sulfides) are developed for the catalytic conversion of soluble polysulfides. A series of literature has presented transition metal compounds and shown their usage benefit for AMSBs.

In this direction, Yang et al.^[172] used titanium-deficient anatase TiO_2 to modify the separator. The deficient TiO_2 helps bind the soluble polysulfides and convert them to the end-discharge product. The detailed electrochemical investigations revealed the enhanced cyclability of the LSB for 1000 cycles with 0.025% capacity fading with the interlayer. The electrochemical performance was

compared with a bare and modified separator with a TiO_2 nondeficient phase. In the other two cases, the trapping and utilization of sulfur are inferior to the cell with a modified interlayer. In the other work by Li et al.^[105] molybdenum oxide (MoO_3) was embedded into the electrospun nanofiber (using polyacrylonitrile) and used as an interlayer to enhance the electrochemical behavior of the LSB. The interlayer also suppresses the dendrite formation on the lithium anode by enabling uniform plating and stripping. The strategy helped the cell to run for 500 charge/discharge cycles with a 0.12% capacity fading rate at 1 C. MoO_3 helps capture and convert the soluble polysulfides; thus, the lithium corrosion and loss of active sulfur are significantly reduced. The other transition metal oxides are explored widely in several research articles. However, the catalytic activity is limited and thus can lead to saturated surfaces after long-term utilization.

Table 3. Summary of the interlayers with heteroatom-doped carbon for LSBs.

S.N.	Cathode	Interlayer	Electrochemical performance Initial reversible capacity/No of cycles/ capacity retention/C rate or current density [mAh g ⁻¹ /n%/C or A g ⁻¹]	Effect of interlayer
1	Bare sulfur ^[164]	Hollow CNT	1072/250/51/0.5	Improvement in specific capacity and cycle performance is observed
2	S/graphene ^[165]	N-doped graphene	733/200/79/0.2	The interlayer improved the cycling performance in terms of reversible capacity, cycle life, and capacity retention
3	S/CNT ^[166]	Sn, N-doped carbon	1123/100/93/0.2	The cell delivers a better specific capacity and cycle stability
4	Bare sulfur ^[167]	S-doped carbon	1544/200/63/0.2	Exhibits a high initial reversible capacity, superior rate capability, and excellent cycling stability
5	Bare sulfur ^[168]	WO ₃ decorated N, S co-doped CNF	1444/100/75/0.2	Shows a superior reversible capacity and rate capabilities
6	Bare sulfur ^[169]	N, S co-doped carbon	1549/300/61/0.1	Initial discharge capacity increased, and cyclic performance also enhanced
7	Bare Sulfur ^[170]	N, P co-doped graphene	1158/500/55/1.0	The cell delivers a better initial capacity, magnificent rate capability, and adequate cycling stability (0.09% capacity decay per cycle)
8	S/CNT ^[171]	N-doped graphene	770/250/79/2.0	Exhibits greater reversible specific capacity, rate capability, and capacity retention

The researchers then moved to another class of transition metal compounds, that is, transition metal-nitrides. Transition metal-nitrides have better electronic conductivity due to nitrogen, which has a lone pair of electrons and acts as a Lewis base. The interaction of nitrides with soluble polysulfides is stronger compared to oxides. Qu et al.^[173] have reported using CNT/sulfur cathode with in situ assembled Si₃N₄/graphene interlayer for LSB. The interaction with the polysulfides was attributed to the presence of Si₃N₄, where N reacts to the cation counterpart forming Li-N, whereas Si reacts with the anion forming the Si—S bond. As a result, the cell operated for 200 cycles at a lower C-rate (0.1 C) with a 0.22% capacity fading rate and 1000 cycles at 1 C with a 0.054% capacity fading rate. Further, the binding energy and adsorption test of Si₃N₄ were calculated with the polysulfides to understand enhanced performance (Figure 12).

In the other work by Chen et al.^[174] Ni-C₃N₄/C modified separator was investigated for LSB. The utilization of the composite enabled the strong absorption of soluble polysulfides, accelerated redox conversion reaction, and fast electron transfer (Figure 13a). As a result, the cell delivered a reversible capacity of 803 mAh g⁻¹ with 89% capacity retention after 300 cycles at 0.5 A g⁻¹. Further, the first-principles calculation verified the enhanced electrochemical property after introducing the interlayer to the LSBs. In the recent work by Ma et al.^[175] Mo₂N quantum dots were decorated over graphene nanosheets and used as interlayers for LSBs. The developed interlayer has sulfophilic and lithiophilic properties, which help reduce the soluble polysulfides' shuttle effect and lithium's dendrite formation. The cell with an interlayer was also tested with the pouch cell configuration and delivered an aerial capacity of 3.89 mAh cm⁻² with a 4.5 mg cm⁻² electrode. The cell was also tested for reduced dendrite formation and showed a stable performance for 1500 h at 5 mA cm⁻².

Huang et al.^[176] designed a hybrid MXene interlayer on a glass fiber separator and demonstrated strong cycling stability, retaining

71% of their capacity after 200 cycles at 1 C for Room-temperature NaSBs. This interlayer consists of a dual-layer design: a bottom layer of large Ti₃C₂T_x nanosheets that physically and chemically restrict polysulfide movement, and a top layer of smaller Mo₂Ti₂C₃T_x flakes that efficiently trap polysulfides and boost their conversion due to high conductivity, surface area, and catalytic activity. These layers effectively confine soluble polysulfides to the cathode side, combining physical blocking, chemical adsorption, and enhanced redox kinetics. This approach offers a promising pathway for building advanced 2D material-based interlayers in next-generation sodium-sulfur batteries. The nitride-based compounds have shown promising performance in the literature for LSBs. However, catalytic behavior is limited as nitride acts only as a perfect binding site for the soluble polysulfides. Transition metal sulfides are explored due to their excellent catalytic behavior toward the soluble polysulfides as another class of materials. The sulfur in the sulfides acts as an active site for the polysulfides to anchor and convert themselves to the thiosulfate complexes. The thiosulfate complex acts as a binding and catalytic site for the upcoming polysulfides. After the interaction, thiosulfate converts to polythionate, forming short-chain (insoluble) polysulfides. In this direction, Seo et al.^[177] have reported using Co_xS_y as hetero-catalysts on carbon nanosheets to serve as an interlayer for LSBs. The prepared interlayer provided superior adsorption of lithium polysulfides. As a result, the cell modified with the interlayer delivered 911 mAh g⁻¹ at 0.2 C after 100 cycles. The enhanced performance was claimed to be the presence of hetero catalysts, which enable the catalytic reduction of soluble polysulfides and conductive carbon nanosheets. Later, Yoon et al.^[120] reported a CoS₂ nanosheet supported on free-standing carbon nanofibers as an interlayer for LSBs. The vertical arrangement of 2D CoS₂ maximizes reactive sites to the electrolyte electrode interface, enabling excellent electrocatalysis. The advantage of using a vertical arrangement is shown in Figure 13b. As a result of the excellent electrocatalytic

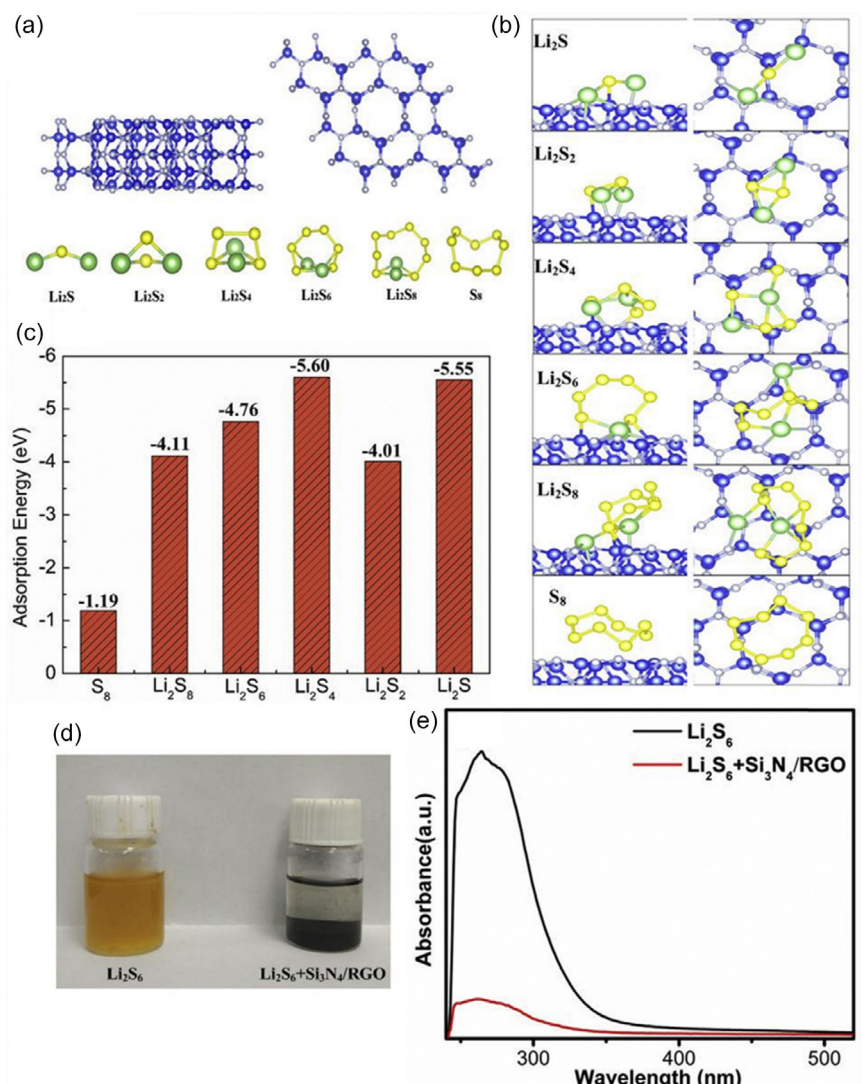


Figure 12. a) Molecular representation of Si_3N_4 supercell and Li_2S_n ($n = 1, 2, 4, 6, 8$) and S_8 clusters. b) Representation of adsorption of Li_2S_n and S_8 clusters on Si_3N_4 , and c) their corresponding adsorption energies. d) Digital photographs of the Li_2S_6 solution (0.02 M in DOL/DME) with (right) and without (left) the $\text{Si}_3\text{N}_4/\text{RGO}$ composite, and e) their corresponding UV-vis absorption spectra of the Li_2S_6 solution with and without the $\text{Si}_3\text{N}_4/\text{RGO}$ composite.^[173] Copyright 2019, Elsevier.^[173]

and electrochemical properties of the as-prepared interlayer, the cell performed for 500 cycles at 1 C, delivering a capacity of 580 mAh g^{-1} .

In addition to oxides, nitrides, and sulfides, transition metal phosphides, selenides, and tellurides have recently emerged as highly promising interlayer materials in LSBs, owing to their superior electrical conductivity, strong chemical affinity toward polysulfides, and intrinsic electrocatalytic activity. These materials often exhibit metal–X (X = P, Se, Te) bonds that facilitate not only strong adsorption of lithium polysulfides but also promote their catalytic conversion to insoluble end products ($\text{Li}_2\text{S}_2/\text{Li}_2\text{S}$), thus minimizing the shuttle effect and improving long-term cycling stability.^[178,179] For example, in a recent study by Anoushka et al.^[180] bifunctional catalytic zinc phosphide (ZnP_2) was used to modify the separator for lithium-sulfur batteries (Figure 14a). Utilizing ZnP_2 not only helped to capture the soluble polysulfides and convert them catalytically to the end discharge product but

also enabled lithium anode stabilization by reducing the anode corrosion and dendrite formation. As a result, the half-cell LSB assembly with this modified separator delivered an initial capacity of 1145 mA h g^{-1} and retained 954 mA h g^{-1} after 100 cycles with an average Coulombic efficiency of 99.8% at 0.1 C. The efficiency of this interlayer was further explored in the full-cell assembly, where it displayed a capacity of 797 mA h g^{-1} and retained 534 mA h g^{-1} after 100 cycles at 0.1 C with a N/P ratio of 3 (Figure 14b). In addition, the pouch cell assembly of LSBs achieved an areal capacity of 1.13 mAh cm^{-2} (Figure 14c). Further, Liqing et al. have reported the use of multitransitional-metal-phosphides [(Mn/Co/Fe)Fe-P] to develop an interlayer for LSBs.^[181] They propose that the (Mn/Co/Fe)Fe-P with a particle size of ≈ 50 nm can effectively anchor soluble polysulfides and enhance the conversion, thereby increasing the sulfur utilization rate. As a result, the LSB with this interlayer could deliver 870 mA h g^{-1} at 3 C with a small capacity decay of

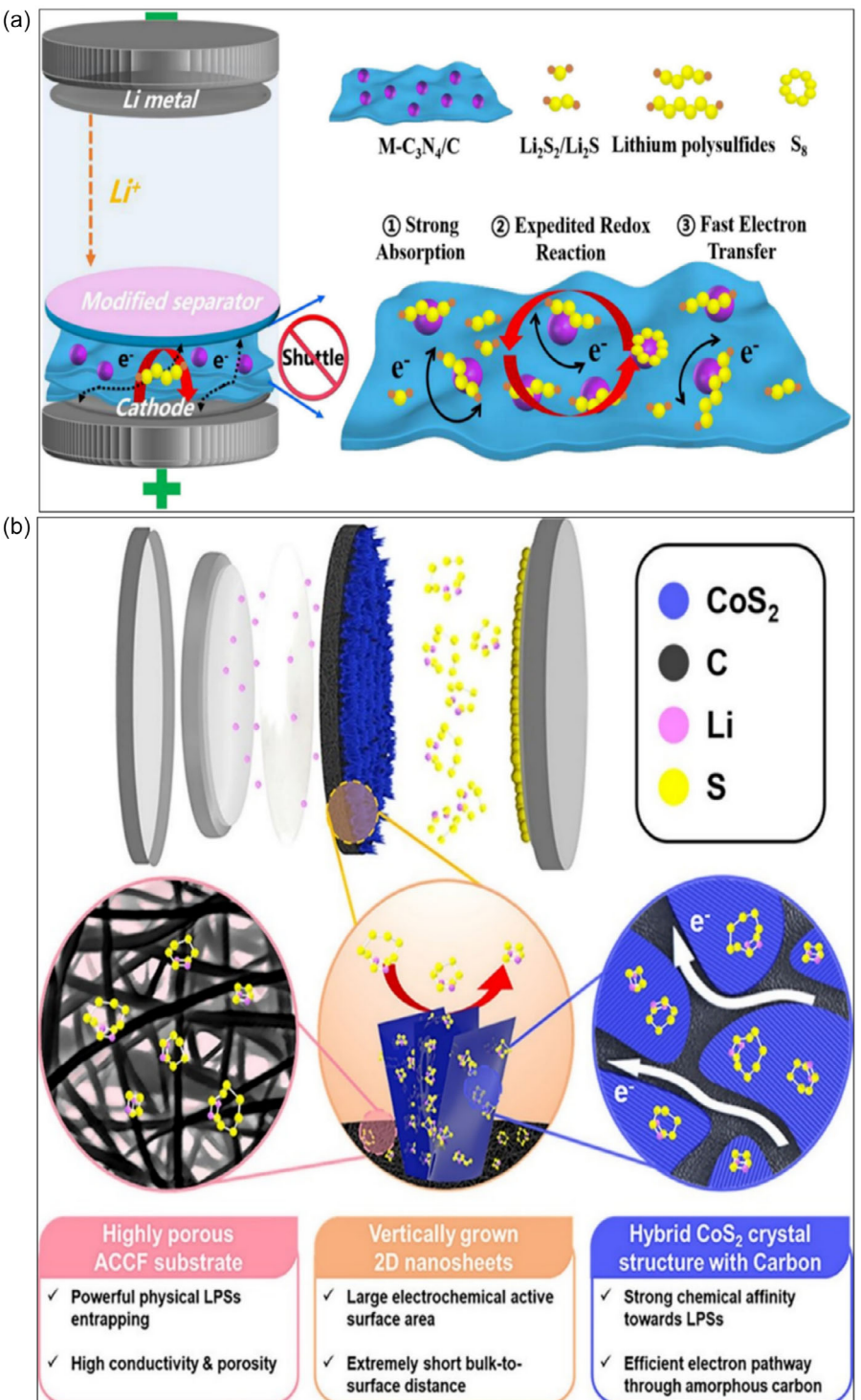


Figure 13. a) Illustration of LSB with $M-C_3N_4/C$ -modified separator and mechanism of polysulfide conversion with reaction kinetics. Reproduced with permission.^[174] Copyright 2020, Elsevier.^[174] b) Advantages of using vertically grown cobalt disulfide and ACCF interlayer for LSB. Reproduced with permission.^[120] Copyright 2021, American Chemical Society.^[120]

0.06% per cycle after 1000 cycles (Figure 14d). In addition, they demonstrated Li^+ plating/stripping behavior for 1000 cycles, revealing reduced Li dendrite formation with the symmetric cell study. The report by Yufeng et al. suggests the use of molybdenum diphosphide (MoP_2) nanoparticles and a CNT film as an interlayer.^[182] MoP_2 can act as a binding and catalytic site for

polysulfide, while CNTs serve as a conductive skeleton to support MoP_2 , ensuring its uniform distribution while anchoring the soluble polysulfides via physisorption, hindering the shuttle effect. Therefore, the cell could deliver 905 mA h g^{-1} over 100 cycles at 0.2 C (Figure 14e,f). Similarly, in a recent study by Yujuan et al.^[183] a mixture of ZIF-67 and melamine was carbonized to synthesize

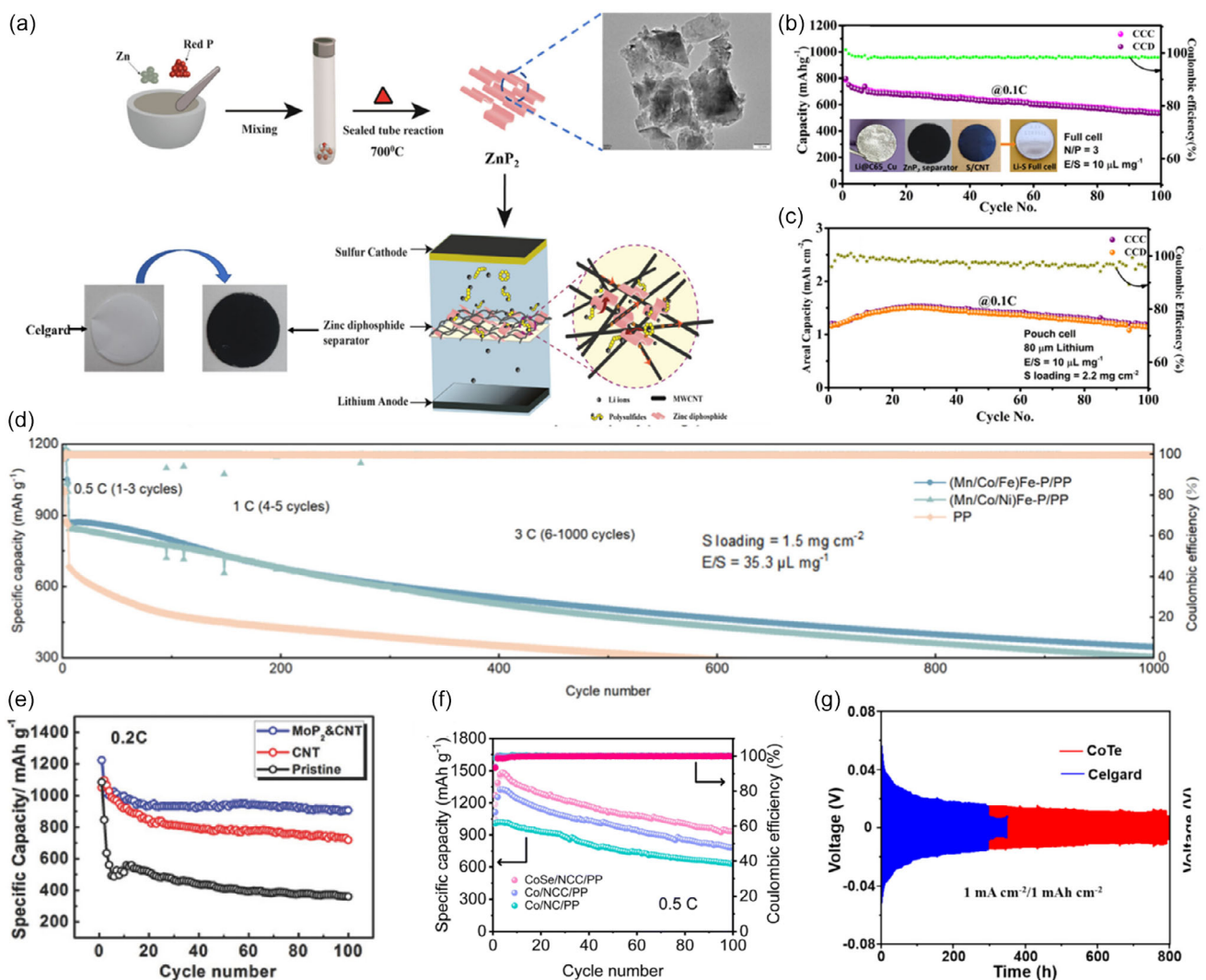


Figure 14. a) Schematic illustration of ZnP₂-modified separator fabrication, b) full-cell cycling at 0.1 C, and c) pouch cell cycling at 0.1 C. Reproduced with permission.^[180] Copyright 2025, American Chemical Society.^[180] d) Cycling performance with (Mn/Co/Fe)Fe-P modified separator at 3 C. Reproduced with permission.^[181] Copyright 2025, American Chemical Society.^[181] e) High plateau capacity contribution and f) low plateau capacity contribution calculated from the discharge capacity of the battery at 0.2 C with MoP₂ and CNT modified separator. Reprinted with permission.^[182] Copyright 2018, Wiley.^[182] g) Plating-stripping profile of lithium symmetric cell with CoTe modified separator. Reprinted with permission.^[184] Copyright 2018, Springer.^[184]

cobalt nanoparticles decorated over N-doped carbon surrounded by carbon nanotubes (Co/NCC). Later, this mixture was in situ selenized to obtain CoSe/NCC to modify the separator for LSBs. The CoSe has sulfurophilic properties, which can enhance the capture ability of polysulfide due to Lewis's acid-base interaction, while NCC can help in maintaining the electronic pathway for efficient electron transfer. Electrochemical investigation revealed excellent performance, delivering 1270 mA h g⁻¹ at 0.5 C and maintaining 73% retention after 100 cycles, illustrating the advantage of this separator. Furthermore, another study by Yao et al.^[184] explored the multifunctional separator decorated with CoTe nanoparticles following vacuum filtration. CoTe nanoparticles showed an effective electrocatalyst characteristic for polysulfide conversion while inhibiting the shuttle effect. In addition, this modified separator regulated the morphology of lithium deposition. This was confirmed by performing the lithium plating/stripping test for 750 h at the current density

of 1 mA cm⁻² (Figure 14g). The electrochemical performance at 1 C revealed a slow capacity decay rate of 0.093% per cycle after 500 cycles. The potential of this modified separator was also investigated at high sulfur loading of 4.6 mg cm⁻² and E/S ratio of 8 μL mg⁻¹, delivering 668 mA h g⁻¹ at 0.5 C. These studies underscore the synergistic effect of combining transition metal chalcogenides/phosphides with carbonaceous support: the metal compound contributes to polysulfide anchoring and conversion, while the carbon scaffold ensures structural stability and conductivity. A detailed summary of transition metal compounds as interlayers and their corresponding electrochemical performance is presented in Table 4.

4.7. Single-Atom Catalysts (SACs)-Doped Carbon Interlayer

In addition to the transition metal compounds, single-atom catalyst (SAC)-doped carbon has been exploited in literature to

S. N.	Cathode	Interlayer	Electrochemical performance Initial reversible capacity/No of cycles/capacity retention/ C-rate [mAh g ⁻¹ /n%/C]
1	Bare sulfur ^[112]	CNT@TiO ₂	783/1000/69/0.5
2	Bare sulfur ^[198]	N-doped SiO ₂	1080/1500/43/1.0
3	Bare sulfur ^[105]	CNF@MoO ₃	1412/500/44/0.5
4	Bare sulfur ^[114]	Carbon@RuO ₂	695/300/96/0.5
5	Bare sulfur ^[199]	CNF@V ₂ O ₅	816/1000/71/3
6	S/ZrO ₂ -hollow CNF ^[200]	Carbon@ZrO ₂	1138/200/77/10
7	Bare sulfur ^[201]	CNT@TiS ₂	1131/300/57/0.2
8	S/carbon nanoparticle ^[202]	Carbon@SnS ₂	1238/200/75/0.2
9	S/graphene ^[203]	VN	1471/100/85/0.2
10	S/rGO ^[204]	Co-NbN-rGO	984/800/41/1.0
11	Bare sulfur ^[180]	ZnP2-CNT	715/1000/61/1.0
12	Bare sulfur ^[181]	[(Mn/Co/Fe) Fe-P]-CNT	870/1000/40/0.5
13	Bare sulfur ^[182]	MoP2-CNT	619/500/88/1.0
14	MWCNT-sulfur ^[183]	CoSe-NCC	874/500/74/1.0
15	S/Ketjen black ^[184]	CoTe-Conductive carbon	735/500/≈48/1.0

improve electrochemical performance. The benefits of using SAC-doped carbon include outstanding catalytic conversion along with excellent electronic conductivity.^[185–187] A variety of SACs have been developed following different synthesis routes, such as coordination design, defect engineering, and spatial confinement.^[115,188,189] Another feature that SACs enable is localized engineering to tune the catalytic behavior toward soluble polysulfides. For instance, Fang et al. reported the decoration of a Co single atom anchored on an N-doped porous carbon (CoSAC-NPC) framework.^[190] The CoSAC-NPC was further blended with N-doped graphene (NG) to further enhance its electronic conductivity and coated on a polypropylene separator following a vacuum filtration technique to use as an interlayer. This interlayer displayed excellent improvement in the electrochemical performance of LSBs owing to its efficient capturing of the soluble polysulfide and catalytic ability. Consequently, the cell with interlayer displayed a capacity of 985 mA h g⁻¹ and retained 788 mA h g⁻¹ after 400 consecutive cycles when investigated at 0.5 C. In another recent report by Mengdi et al. a functional nanofibrous free-standing interlayer was reported to anchor iron and zinc single atoms to serve as a shuttle effect barrier and kinetics promoter.^[191] Benefiting from the excellent electronic conductivity with the interwoven network of carbon nanofibers and excellent catalytic activity to Fe and Zn, the interlayer demonstrated superior enhancement in the electrochemical performance. The LSB with this modified interlayer exhibited an initial capacity of 1140 mA h g⁻¹ while retaining 618 mA h g⁻¹ after 600 cycles at 1 C. This strategy has shown significant improvement in the electrochemical performance; however, very few reports are available where they are explored for the interlayer application. In addition, this approach is yet to be explored in the NaSBs and KSBs chemistries.

5. Outlook and Perspective

The ongoing quest for next-generation energy storage systems is increasingly focused on technologies that transcend the performance limitations of commercial LIBs. Among the promising alternatives, AMSBs—including LSB, NaSB, and KSB chemistries—stand out due to their potential to deliver: 1) lower manufacturing costs, 2) greater elemental abundance in Earth's crust, and 3) significantly higher energy densities, with some configurations offering up to twice the capacity of LIBs. However, despite their promise, AMSBs face intrinsic challenges such as the insulating nature of sulfur, substantial volume fluctuations during cycling, and the notorious polysulfide shuttle effect, all of which hinder long-term performance and commercialization.

Encouraging progress has been made in the commercialization of LSBs, driven by innovation from industry leaders like PolyPlus Battery Company, NexTech Batteries Inc., Lyten Inc., and Zeta Energy LLC. However, NaSBs and KSBs remain limited by poor electrochemical performance, primarily due to severe polysulfide shuttling, which compromises cycle life and Coulombic efficiency. Overcoming these challenges demands novel design strategies tailored to the unique chemistry of each system.

One such strategy involves the integration of interlayers, which have already shown significant promise in LSBs but remain underexplored in other AMSB variants. Interlayers can trap migrating polysulfide species, mitigate active material loss, and suppress dendrite growth, ultimately improving both stability and cycle life. This perspective explores the role of interlayers in AMSBs and outlines a rational design approach for next-generation systems.

5.1. Classification of Interlayers

Interlayers serve as protective barriers that limit the detrimental migration of soluble polysulfides during battery operation. Depending on their placement within the cell, interlayers are classified into two types: 1) anodic interlayers—positioned adjacent to the anode, either as a freestanding film or as a coating on the separator. These interlayers act as a barrier against polysulfide diffusion into the anode region, thereby preventing corrosion, facilitating uniform metal ion deposition, and suppressing dendrite formation. This configuration also enhances the structural integrity of the cell and prolongs its operational life; 2) cathodic interlayers—placed facing the cathode, these interlayers help trap and re-anchor diffusing polysulfide species within the cathodic region, allowing for their reutilization in subsequent cycles. This retention boosts sulfur utilization and contributes to improved capacity retention and extended cycle life.

5.2. Bare Carbon-Based Interlayers

Carbon-based materials have long been employed in energy storage due to their high surface area, tunable porosity, and environmental sustainability. However, when used as bare interlayers in AMSBs, their ability to absorb polysulfides is inherently limited.

The physical adsorption capacity saturates over extended cycling, reducing the effectiveness of the interlayer and ultimately compromising long-term performance. Consequently, while simple to fabricate, bare carbon interlayers are suboptimal for ensuring robust polysulfide management over prolonged use.

5.3. Heteroatom-Doped Carbon-Based Interlayers

Heteroatom doping (e.g., N, S, O, B, P) enhances the chemical affinity of carbon structures for polar polysulfide species by introducing localized polarity and active sites. These dopants create stronger interactions, such as electrostatic forces or Lewis's acid–base bonding, leading to improved polysulfide anchoring.

However, the interactions are often irreversible, leading to polysulfide accumulation and eventual performance decay. While introducing sulfur moieties can offer some catalytic activity, the effect is limited by the necessary tradeoff between doping concentration and electrical conductivity. Thus, although superior to bare carbon, this strategy alone may not suffice for high-performance AMSBs.

5.4. Transition Metal Compound–Carbon Composite Interlayers

Transition metal compounds (e.g., TiO₂, Mn₂O₃, V₂O₅, MoS₂, TiS₂, VN) bring catalytic capabilities to interlayer design. These materials can chemically bind and catalytically convert soluble long-chain polysulfides into shorter, more stable species, enhancing sulfur utilization and minimizing shuttle-related losses.

When integrated into a carbon matrix, carbon serves as a conductive host while the transition metal compounds facilitate chemical transformations. The formation of intermediate complexes (e.g., thiosulfates) during redox cycling further supports catalytic conversion, resulting in improved redox kinetics and extended cycle life. Optimal performance is typically observed when the metal compound loading is kept below 10 wt%, ensuring catalytic efficiency without compromising electronic conductivity.

5.5. Single-Atom Catalyst (SAC)–Carbon Composite Interlayers

An emerging frontier in interlayer design involves single-atom catalysts (SACs), such as Co, Ni, or Fe, embedded within carbon matrices. SACs exhibit exceptional catalytic activity due to their maximum atom utilization and unique electronic structures, making them highly effective in promoting polysulfide conversion reactions. Incorporating SACs into interlayers not only enhances sulfur utilization and redox kinetics but also suppresses dendritic growth and boosts electrochemical stability. This approach represents a cutting-edge solution for improving AMSB performance while maintaining a lightweight and electrically conductive scaffold.

5.6. Toward Practical AMSB Devices with Interlayers

Despite their benefits, interlayers are typically considered inactive components, as they do not directly participate in electrochemical

energy conversion. Their added mass can negatively affect the gravimetric energy density of the overall system. Therefore, for real-world applications, it is critical to engineer ultra-thin, lightweight interlayers that combine physical polysulfide confinement with chemical/catalytic activity.

Future research should prioritize the following: 1) minimizing interlayer thickness while maintaining mechanical integrity, 2) maximizing polysulfide trapping efficiency, and 3) integrating catalytic functionalities to accelerate redox reactions.

By optimizing interlayer design along these lines, AMSBs can be transformed from laboratory curiosities into commercially viable energy storage solutions, aligning with the global demand for safer, more sustainable, and higher-performing batteries.

Acknowledgements

V.K.B. acknowledges the Ministry of Education (MoE, India) for financial support under the Prime Minister's Research Fellowship (PMRF). C.S.S. acknowledges the SERB and DST SwarnaJayanti Fellowship for partial financial assistance.

Conflict of Interest

The authors declare no conflict of interest.

Author Contributions

Vikram Kishore Bharti: conceptualization, writing—original draft, writing review, and editing. **Ashish Priyam Goswami:** writing—original draft, writing review, and editing. **Mudrika Khandelwal:** conceptualization, supervision, writing review, and editing. **Chandra Shekhar Sharma:** conceptualization, supervision, writing review, and editing. **Vikram Kishore Bharti and Ashish Priyam Goswami** contributed equally to this work.

Keywords: alkali metal–sulfur batteries • carbon • interlayers • next-generation energy storage • shuttle effects

- [1] M. Armand, J.-M. Tarascon, *Nature* **2008**, *451*, 652.
- [2] B. Dunn, H. Kamath, J.-M. Tarascon, *Science* **2011**, *334*, 928.
- [3] R. Fang, S. Zhao, D.-W. Wang, Z. Sun, H.-M. Cheng, F. Li, *ACS Appl. Energy Mater.* **2019**, *2*, 7393.
- [4] J.-M. Tarascon, M. Armand, *Nature* **2001**, *414*, 359.
- [5] J. B. Goodenough, K.-S. Park, *J. Am. Chem. Soc.* **2013**, *135*, 1167.
- [6] A. Manthiram, B. Song, W. Li, *Energy Storage Mater.* **2017**, *6*, 125.
- [7] W. Li, B. Song, A. Manthiram, *Chem. Soc. Rev.* **2017**, *46*, 3006.
- [8] M. Li, J. Lu, Z. Chen, K. Amine, *Adv. Mater.* **2018**, *30*, 1800561.
- [9] N. Choi, Z. Chen, S. A. Freunberger, X. Ji, Y. Sun, K. Amine, G. Yushin, L. F. Nazar, J. Cho, P. G. Bruce, *Angew. Chem., Int. Ed.* **2012**, *51*, 9994.
- [10] K. Amine, I. Belharouak, Z. Chen, T. Tran, H. Yumoto, N. Ota, S.-T. Myung, Y.-K. Sun, *Adv. Mater.* **2010**, *22*, 3052.
- [11] V. K. Bharti, A. P. Goswami, C. S. Sharma, M. Khandelwal, *J. Electroanal. Chem.* **2024**, *957*, 118142.
- [12] P. G. Bruce, S. A. Freunberger, L. J. Hardwick, J.-M. Tarascon, *Nat. Mater.* **2012**, *11*, 19.
- [13] J. W. Choi, D. Aurbach, *Nat. Rev. Mater.* **2016**, *1*, 1.
- [14] X. Shen, H. Liu, X.-B. Cheng, C. Yan, J.-Q. Huang, *Energy Storage Mater.* **2018**, *12*, 161.

- [15] Y. Mekonnen, A. Sundararajan, A. I. Sarwat, *SoutheastCon*, Norfolk, VA, USA 2016, 1.
- [16] S. Ahmed, P. A. Nelson, K. G. Gallagher, N. Susarla, D. W. Dees, *J. Power Sources* 2017, 342, 733.
- [17] B. E. Murdock, K. E. Toghill, N. Tapia-Ruiz, *Adv. Energy Mater.* 2021, 11, 2102028.
- [18] P. Albertus, S. Babinec, S. Litzelman, A. Newman, *Nat. Energy* 2018, 3, 16.
- [19] R. Schmuck, R. Wagner, G. Höppl, T. Placke, M. Winter, *Nat. Energy* 2018, 3, 267.
- [20] M. Zhang, W. Chen, L. Xue, Y. Jiao, T. Lei, J. Chu, J. Huang, C. Gong, C. Yan, Y. Yan, Y. Hu, X. Wang, J. Xiong, *Adv. Energy Mater.* 2020, 10, 1903008.
- [21] Y. Hu, W. Chen, T. Lei, Y. Jiao, J. Huang, A. Hu, C. Gong, C. Yan, X. Wang, J. Xiong, *Adv. Energy Mater.* 2020, 10, 2000082.
- [22] M. Salama, R. Attias, B. Hirsch, R. Yemini, Y. Gofer, M. Noked, D. Aurbach, *ACS Appl. Mater. Interfaces* 2018, 10, 36910.
- [23] W. Weng, J. Xiao, Y. Shen, X. Liang, T. Lv, W. Xiao, *Angew. Chem., Int. Ed.* 2021, 60, 24905.
- [24] A. P. Goswami, V. K. Bharti, C. S. Sharma, M. Khandelwal, *Carbon Trends* 2024, 16, 100391.
- [25] E. Ghasemiestahbanati, A. Shehzad, K. Konstas, C. J. Setter, L. A. O'Dell, M. Shaibani, M. Majumder, M. R. Hill, *J. Mater. Chem. A* 2022, 10, 902.
- [26] Y. Li, P. Zhou, H. Li, T. Gao, L. Zhou, Y. Zhang, N. Xiao, Z. Xia, L. Wang, Q. Zhang, L. Gu, S. Guo, *Small Methods* 2020, 4, 1900701.
- [27] L. Chen, L. L. Shaw, *J. Power Sources* 2014, 267, 770.
- [28] Y.-S. Su, A. Manthiram, *Chem. Commun.* 2012, 48, 8817.
- [29] L. Chen, H. Yu, W. Li, M. Dirican, Y. Liu, X. Zhang, *J. Mater. Chem. A* 2020, 8, 10709.
- [30] S.-H. Chung, R. Singhal, V. Kalra, A. Manthiram, *J. Phys. Chem. Lett.* 2015, 6, 2163.
- [31] L.-L. Kong, Z. Zhang, Y.-Z. Zhang, S. Liu, G.-R. Li, X.-P. Gao, *ACS Appl. Mater. Interfaces* 2016, 8, 31684.
- [32] T. Zhuang, J. Huang, H. Peng, L. He, X. Cheng, C. Chen, Q. Zhang, *Small* 2016, 12, 381.
- [33] V. K. Bharti, C. S. Sharma, M. Khandelwal, *Carbon* 2023, 212, 118173.
- [34] X. Tang, D. Zhou, P. Li, X. Guo, B. Sun, H. Liu, K. Yan, Y. Gogotsi, G. Wang, *Adv. Mater.* 2020, 32, 1906739.
- [35] P. Xiong, X. Han, X. Zhao, P. Bai, Y. Liu, J. Sun, Y. Xu, *ACS Nano* 2019, 13, 2536.
- [36] N.-C. Lai, G. Cong, Y.-C. Lu, *J. Mater. Chem. A* 2019, 7, 20584.
- [37] J.-L. Qin, B.-Q. Li, J.-Q. Huang, L. Kong, X. Chen, H.-J. Peng, J. Xie, R. Liu, Q. Zhang, *Mater. Chem. Front.* 2019, 3, 615.
- [38] W. Kong, L. Yan, Y. Luo, D. Wang, K. Jiang, Q. Li, S. Fan, J. Wang, *Adv. Funct. Mater.* 2017, 27, 1606663.
- [39] B. Zheng, N. Li, J. Yang, J. Xi, *Chem. Commun.* 2019, 55, 2289.
- [40] L. Jiao, C. Zhang, C. Geng, S. Wu, H. Li, W. Lv, Y. Tao, Z. Chen, G. Zhou, J. Li, G. Ling, Y. Wan, Q. Yang, *Adv. Energy Mater.* 2019, 9, 1900219.
- [41] X. Zhao, Y. Lu, Z. Qian, R. Wang, Z. Guo, *EcoMat* 2020, 2, e12038.
- [42] R. Xiao, K. Chen, X. Zhang, Z. Yang, G. Hu, Z. Sun, H.-M. Cheng, F. Li, *J. Energy Chem.* 2021, 54, 452.
- [43] M. Salama, R. Attias, R. Yemini, Y. Gofer, D. Aurbach, M. Noked, *ACS Energy Lett.* 2019, 4, 436.
- [44] H. Ye, Y. Li, *InfoMat* 2022, 4, e12291.
- [45] L. Medenbach, P. Adelhelm, in *Electrochemical Energy Storage* (Ed: R.-A. Eichel), Topics in Current Chemistry Collections, Springer International Publishing, Cham 2019, pp. 101–125.
- [46] X. Hong, J. Mei, L. Wen, Y. Tong, A. J. Vasileff, L. Wang, J. Liang, Z. Sun, S. X. Dou, *Adv. Mater.* 2019, 31, 1802822.
- [47] A. Gangadharan, S. Mamidi, C. S. Sharma, T. N. Rao, *Mater. Today Commun.* 2020, 23, 100926.
- [48] M. P. Illa, A. D. Pathak, C. S. Sharma, M. Khandelwal, *ACS Appl. Energy Mater.* 2020, 3, 8676.
- [49] V. K. Bharti, A. D. Pathak, C. S. Sharma, M. Khandelwal, *Electrochim. Acta* 2022, 422, 140531.
- [50] V. K. Bharti, S. K. Cherian, M. M. Gaikwad, A. D. Pathak, C. S. Sharma, *Lithium-Sulfur Batteries*, Elsevier 2022, pp. 37–55.
- [51] V. K. Bharti, A. D. Pathak, C. S. Sharma, M. Khandelwal, *Carbohydr. Polym.* 2022, 293, 119731.
- [52] G. Singh, R. Bahadur, J. M. Lee, I. Y. Kim, A. M. Ruban, J. M. Davidraj, D. Semit, A. Karakoti, H. Ala'a, A. Vinu, *Chem. Eng. J.* 2021, 406, 126787.
- [53] Q. Zhao, Y. Hu, K. Zhang, J. Chen, *Inorg. Chem.* 2014, 53, 9000.
- [54] Z. Li, Y. Huang, L. Yuan, Z. Hao, Y. Huang, *Carbon* 2015, 92, 41.
- [55] Y. Dai, C. Xu, X. Liu, X. He, Z. Yang, W. Lai, L. Li, Y. Qiao, S. Chou, *Carbon Energy* 2021, 3, 253.
- [56] J. Luo, K. Wang, Y. Qian, P. Wang, H. Yuan, O. Sheng, B. Li, H. Wang, Y. Wang, Y. Liu, *Nano Energy* 2023, 118, 108958.
- [57] Q. Gou, L. Lu, S. Lin, W. Zhang, Y. R. Ayillon, Z. Zhou, L. Zhu, Y. Lu, *Macromol. Rapid Commun.* 2025, 46, 2500155.
- [58] Y. Chen, C. Ma, Z. Li, T. Zhang, C. Li, J. Niu, S. Yao, *Electrochim. Acta* 2025, 517, 145762.
- [59] Y. Wang, E. Indubala, C. Ma, C. Zhang, L. Xiao, B. Lv, S. Yao, *J. Energy Storage* 2025, 121, 116575.
- [60] S. Li, J. Warzywoda, S. Wang, G. Ren, Z. Fan, *Carbon* 2017, 124, 212.
- [61] J. Liu, H. Zhang, B. Xie, J. Cheng, T. Song, Y. Bai, R. Ma, C. M. Li, *Chem. Eng. J.* 2025, 510, 161470.
- [62] F. Liu, M. Yuan, P. Feng, S. Yu, Z. Hu, H. Xiang, M. Zhu, *Int. J. Biol. Macromol.* 2025, 304, 140813.
- [63] T. Zhou, Y. Zhu, X. Huang, T. Han, J. Liu, *Chem. Commun.* 2025, 61, 7035.
- [64] N. Badi, A. S. Roy, H. A. Al-Aoh, S. A. Alghamdi, A. S. Alatawi, A. A. Alatawi, A. Ignatiev, *Mater. Sci. Energy Technol.* 2023, 6, 351.
- [65] Z. Wang, J. Cheng, W. Ni, L. Gao, D. Yang, J. M. Razal, B. Wang, *J. Power Sources* 2017, 342, 772.
- [66] X. Chen, C. Zhao, K. Yang, S. Sun, J. Bi, N. Zhu, Q. Cai, J. Wang, W. Yan, *Energy Environ. Mater.* 2023, 6, e12483.
- [67] S. Li, W. Zhang, J. Zheng, M. Lv, H. Song, L. Du, *Adv. Energy Mater.* 2021, 11, 2000779.
- [68] Y. Huang, L. Lin, C. Zhang, L. Liu, Y. Li, Z. Qiao, J. Lin, Q. Wei, L. Wang, Q. Xie, D. Peng, *Adv. Sci.* 2022, 9, 2106004.
- [69] W. Ren, W. Ma, S. Zhang, B. Tang, *Energy Storage Mater.* 2019, 23, 707.
- [70] J. Wang, H. Wang, S. Jia, Q. Zhao, Q. Zheng, Y. Ma, T. Ma, X. Li, *J. Energy Storage* 2023, 72, 108372.
- [71] Y. V. Mikhaylik, J. R. Akridge, *J. Electrochem. Soc.* 2004, 151, A1969.
- [72] W. Chen, T. Lei, W. Lv, Y. Hu, Y. Yan, Y. Jiao, W. He, Z. Li, C. Yan, J. Xiong, *Adv. Mater.* 2018, 30, 1804084.
- [73] X. Song, T. Gao, S. Wang, Y. Bao, G. Chen, L.-X. Ding, H. Wang, *J. Power Sources* 2017, 356, 172.
- [74] D. S. Wu, F. Shi, G. Zhou, C. Zu, C. Liu, K. Liu, Y. Liu, J. Wang, Y. Peng, Y. Cui, *Energy Storage Mater.* 2018, 13, 241.
- [75] G. Zhou, H. Tian, Y. Jin, X. Tao, B. Liu, R. Zhang, Z. W. Seh, D. Zhuo, Y. Liu, J. Sun, J. Zhao, C. Zu, D. S. Wu, Q. Zhang, Y. Cui, *Proc. Natl. Acad. Sci.* 2017, 114, 840.
- [76] H.-J. Peng, Z.-W. Zhang, J.-Q. Huang, G. Zhang, J. Xie, W.-T. Xu, J.-L. Shi, X. Chen, X.-B. Cheng, Q. Zhang, *Adv. Mater.* 2016, 28, 9551.
- [77] X. Fan, L. Chen, O. Borodin, X. Ji, J. Chen, S. Hou, T. Deng, J. Zheng, C. Yang, S.-C. Liou, *Nat. Nanotechnol.* 2018, 13, 715.
- [78] H. Peng, G. Zhang, X. Chen, Z. Zhang, W. Xu, J. Huang, Q. Zhang, *Angew. Chem., Int. Ed.* 2016, 55, 12990.
- [79] W. Kong, L. Yan, Y. Luo, D. Wang, K. Jiang, Q. Li, S. Fan, J. Wang, *Adv. Funct. Mater.* 2017, 27, 1606663.
- [80] J. Hwang, H. M. Kim, S. Lee, J. Lee, A. Abouimrane, M. A. Khaleel, I. Belharouak, A. Manthiram, Y. Sun, *Adv. Energy Mater.* 2016, 6, 1501480.
- [81] X. Yuan, L. Wu, X. He, K. Zeinu, L. Huang, X. Zhu, H. Hou, B. Liu, J. Hu, J. Yang, *Chem. Eng. J.* 2017, 320, 178.
- [82] S. Bai, X. Liu, K. Zhu, S. Wu, H. Zhou, *Nat. Energy* 2016, 1, 1.
- [83] Y. Zhou, G. Hu, W. Zhang, Q. Li, Z. Zhao, Y. Zhao, F. Li, F. Geng, *Energy Storage Mater.* 2017, 9, 39.
- [84] J. Liang, Z.-H. Sun, F. Li, H.-M. Cheng, *Energy Storage Mater.* 2016, 2, 76.
- [85] L. Wang, Z. Zhou, X. Yan, F. Hou, L. Wen, W. Luo, J. Liang, S. X. Dou, *Energy Storage Mater.* 2018, 14, 22.
- [86] P. Adelhelm, P. Hartmann, C. L. Bender, M. Busche, C. Eufinger, J. Janek, *Beilstein J. Nanotechnol.* 2015, 6, 1016.
- [87] W. Yao, K. Liao, T. Lai, H. Sul, A. Manthiram, *Chem. Rev.* 2024, 124, 4935.
- [88] N. Nitta, F. Wu, J. T. Lee, G. Yushin, *Mater. Today* 2015, 18, 252.
- [89] Z. W. Seh, Y. Sun, Q. Zhang, Y. Cui, *Chem. Soc. Rev.* 2016, 45, 5605.
- [90] A. Manthiram, Y. Fu, S.-H. Chung, C. Zu, Y.-S. Su, *Chem. Rev.* 2014, 114, 11751.
- [91] M. Chen, M. Shao, J. Jin, L. Cui, H. Tu, X. Fu, *Energy Storage Mater.* 2022, 47, 629.
- [92] R. Pai, V. Kalra, *ACS Appl. Energy Mater.* 2021, 4, 5649.
- [93] R. Ma, L. Fan, J. Wang, B. Lu, *Electrochim. Acta* 2019, 293, 191.
- [94] J. Ma, J. Fan, S. Chen, X. Yang, K. N. Hui, H. Zhang, C. W. Bielawski, J. Geng, *ACS Appl. Mater. Interfaces* 2019, 11, 13234.
- [95] S. Yao, R. Guo, F. Xie, Z. Wu, K. Gao, C. Zhang, X. Shen, T. Li, S. Qin, *Electrochim. Acta* 2020, 337, 135765.
- [96] J.-Y. Hwang, H. M. Kim, C. S. Yoon, Y.-K. Sun, *ACS Energy Lett.* 2018, 3, 540.
- [97] X. Yu, A. Manthiram, *Adv. Funct. Mater.* 2020, 30, 2004084.
- [98] S. Chung, A. Manthiram, *Adv. Mater.* 2019, 31, 1901125.
- [99] N. Lingappan, W. Lee, S. Passerini, M. Pecht, *Renewable Sustainable Energy Rev.* 2023, 187, 113726.
- [100] Y. Song, L. Sheng, L. Wang, H. Xu, X. He, *Electrochim. Commun.* 2021, 124, 106948.

- [101] A. Bhargav, J. He, A. Gupta, A. Manthiram, *Joule* **2020**, *4*, 285.
- [102] S. S. Zhang, *Energies* **2012**, *5*, 5190.
- [103] X. Fan, Y. Liu, J. Tan, S. Yang, X. Zhang, B. Liu, H. Cheng, Z. Sun, F. Li, *J. Mater. Chem. A* **2022**, *10*, 7653.
- [104] M. S. Klia, O. Eroglu, H. Kizil, *J. Appl. Polym. Sci.* **2020**, *137*, 48606.
- [105] H. Li, X. Wang, C. Qi, C. Zhao, C. Fu, L. Wang, T. Liu, *Phys. Chem. Chem. Phys.* **2020**, *22*, 2157.
- [106] Y. Li, L. Meng, L. Jin, L. Yun, H. Jian, *Mater. Res. Express* **2020**, *6*, 125547.
- [107] W. Yang, Z. Ni, B. Deng, J. Hou, R. Huang, D. You, K. Wei, Y. Zhang, X. Li, Y. Zhang, *Ceram. Int.* **2022**, *48*, 37287.
- [108] L. Fan, M. Li, X. Li, W. Xiao, Z. Chen, J. Lu, *Joule* **2019**, *3*, 361.
- [109] Y. Huang, D. Lv, Z. Zhang, Y. Ding, F. Lai, Q. Wu, H. Wang, Q. Li, Y. Cai, Z. Ma, *Chem. Eng. J.* **2020**, *387*, 124122.
- [110] J. Wu, X. Li, H. Zeng, Y. Xue, F. Chen, Z. Xue, Y. Ye, X. Xie, *J. Mater. Chem. A* **2019**, *7*, 7897.
- [111] J. Li, Z. Xiong, Y. Wu, H. Li, X. Liu, H. Peng, Y. Zheng, Q. Zhang, Q. Iron Liu, *J. Energy Chem.* **2022**, *73*, 513.
- [112] L. Yang, G. Li, X. Jiang, T. Zhang, H. Lin, J. Y. Lee, *J. Mater. Chem. A* **2017**, *5*, 12506.
- [113] X. Tao, J. Wang, Z. Ying, Q. Cai, G. Zheng, Y. Gan, H. Huang, Y. Xia, C. Liang, W. Zhang, Y. Cui, *Nano Lett.* **2014**, *14*, 5288.
- [114] J. Balach, T. Jaumann, S. Mühlhoff, J. Eckert, L. Giebel, *Chem. Commun.* **2016**, *52*, 8134.
- [115] Z. Zou, Q. Wang, J. Yan, K. Zhu, K. Ye, G. Wang, D. Cao, *ACS Nano* **2021**, *15*, 12140.
- [116] S. Chen, G. Li, Z. Zhu, R. Zhu, J. Zhang, Y. Yue, G. Li, L. Zhou, Z. Yan, *J. Energy Chem.* **2025**, *107*, 440.
- [117] A.-G. Nguyen, R. Verma, in *Atomically Precise Electrocatalysts for Electrochemical Energy Applications* (Eds: A. Kumar, R. K. Gupta), Springer Nature Switzerland, Cham **2024**, pp. 383–402.
- [118] J. Zhou, T. Wu, X. Zhou, J. Xi, *Phys. Chem. Chem. Phys.* **2022**, *24*, 17383.
- [119] T. Wang, K. Kretschmer, S. Choi, H. Pang, H. Xue, G. Wang, *Small Methods* **2017**, *1*, 1700089.
- [120] H. Yoon, D. Park, H. J. Song, S. Park, D.-W. Kim, *ACS Sustainable Chem. Eng.* **2021**, *9*, 8487.
- [121] J. Zhu, Y. Liu, L. Zhong, J. Wang, H. Chen, S. Zhao, Y. Qiu, *J. Electroanal. Chem.* **2021**, *881*, 114950.
- [122] Y. Zhu, X. Wu, M. Li, Y. Ji, Q. Li, X. He, Z. Lei, Z. Liu, R. Jiang, J. Sun, *ACS Sustainable Chem. Eng.* **2022**, *10*, 776.
- [123] S. Zhang, H. Shi, J. Tang, W. Shi, Z.-S. Wu, X. Wang, *Sci. China Mater.* **2021**, *64*, 2949.
- [124] Q. Xie, J. Zhang, P. Zhao, *J. Electroanal. Chem.* **2021**, *898*, 115629.
- [125] Y. Mo, J. Lin, S. Li, J. Yu, *Chem. Eng. J.* **2022**, *433*, 134306.
- [126] K. Zou, N. Li, X. Dai, W. Jing, M. Shi, C. Lu, Q. Tan, Y. Xin, J. Sun, Y. Chen, Y. Liu, *ACS Appl. Nano Mater.* **2020**, *3*, 5732.
- [127] Z. Sun, Y. Guo, B. Li, T. Tan, Y. Zhao, *Solid State Sci.* **2019**, *95*, 105924.
- [128] J.-Q. Huang, Z.-L. Xu, S. Abouali, M. A. Garakani, J.-K. Kim, *Carbon* **2016**, *99*, 624.
- [129] G. Ma, Z. Wen, J. Jin, M. Wu, X. Wu, J. Zhang, *J. Power Sources* **2014**, *267*, 542.
- [130] L. Yin, H. Dou, A. Wang, G. Xu, P. Nie, Z. Chang, X. Zhang, *New J. Chem.* **2018**, *42*, 1431.
- [131] G. Ma, Z. Wen, Q. Wang, C. Shen, P. Peng, J. Jin, X. Wu, *J. Power Sources* **2015**, *273*, 511.
- [132] H. Zhong, L. Zhang, *Mater. Lett.* **2022**, *310*, 131499.
- [133] H. M. Kim, J.-Y. Hwang, A. Manthiram, Y.-K. Sun, *ACS Appl. Mater. Interfaces* **2016**, *8*, 983.
- [134] S. Chung, A. Manthiram, *Adv. Mater.* **2014**, *26*, 1360.
- [135] R. Chen, Y. Zhou, X. Li, *Nano Lett.* **2022**, *22*, 1217.
- [136] S. Azam, Z. Wei, R. Wang, *J. Colloid Interface Sci.* **2022**, *615*, 417.
- [137] N. Wei, J. Cai, R. Wang, M. Wang, W. Lv, H. Ci, J. Sun, Z. Liu, *Nano Energy* **2019**, *66*, 104190.
- [138] B. Xu, Y. Zhao, H. Liu, S. Cheng, J. Liu, F. Meng, *Mater. Lett.* **2021**, *305*, 130753.
- [139] M. E. Pam, S. Huang, S. Fan, D. Geng, D. Kong, S. Chen, M. Ding, L. Guo, L. K. Ang, H. Y. Yang, *Mater. Today Energy* **2020**, *16*, 100380.
- [140] Q. Lin, B. Ding, S. Chen, P. Li, Z. Li, Y. Shi, H. Dou, X. Zhang, *ACS Appl. Energy Mater.* **2020**, *3*, 11206.
- [141] R. Yi, C. Liu, Y. Zhao, L. J. Hardwick, Y. Li, X. Geng, Q. Zhang, L. Yang, C. Zhao, *Electrochim. Acta* **2019**, *299*, 479.
- [142] Z. Nie, H. Zhang, Y. Lu, C. Han, Y. Du, Z. Sun, Y. Yan, H. Yu, X. Zhang, J. Zhu, *Chem. Eng. J.* **2021**, *409*, 128137.
- [143] N. Li, L. Yu, J. Yang, B. Zheng, X. Qiu, J. Xi, *Nano Energy* **2021**, *79*, 105466.
- [144] J. Park, J. Moon, V. Ri, S. Lee, C. Kim, E. J. Cairns, *ACS Appl. Energy Mater.* **2021**, *4*, 3518.
- [145] X. Wang, Y. Zhao, F. Wu, S. Liu, Z. Zhang, Z. Tan, X. Du, J. Li, *J. Energy Chem.* **2021**, *57*, 19.
- [146] J. Balach, T. Jaumann, M. Klose, S. Oswald, J. Eckert, L. Giebel, *Adv. Funct. Mater.* **2015**, *25*, 5285.
- [147] H. Zhao, H. Mo, P. Mao, R. Ran, W. Zhou, K. Liao, *ACS Appl. Mater. Interfaces* **2024**, *16*, 68772.
- [148] Y. Hwa, E. Yi, H. Shen, Y. Sung, J. Kou, K. Chen, D. Y. Parkinson, M. M. Doeff, E. J. Cairns, *Nano Lett.* **2019**, *19*, 4731.
- [149] V. K. Bharti, A. Gangadharan, S. K. Kumar, A. D. Pathak, C. S. Sharma, *Mater. Adv.* **2021**, *2*, 3031.
- [150] V. Bharti, A. Gangadharan, T. N. Rao, C. S. Sharma, *Mater. Today Commun.* **2020**, *22*, 100717.
- [151] J.-Q. Huang, B. Zhang, Z.-L. Xu, S. Abouali, M. A. Garakani, J. Huang, J.-K. Kim, *J. Power Sources* **2015**, *285*, 43.
- [152] M. Manoj, M. Jasna, K. M. Anilkumar, A. Abhilash, B. Jinisha, V. S. Pradeep, S. Jayalekshmi, *Appl. Surf. Sci.* **2018**, *458*, 751.
- [153] R. Singhal, S.-H. Chung, A. Manthiram, V. Kalra, *J. Mater. Chem. A* **2015**, *3*, 4530.
- [154] L. Yan, N. Luo, W. Kong, S. Luo, H. Wu, K. Jiang, Q. Li, S. Fan, W. Duan, J. Wang, *J. Power Sources* **2018**, *389*, 169.
- [155] P. Cheng, P. Guo, D. Liu, Y. Wang, K. Sun, Y. Zhao, D. He, *J. Alloys Compd.* **2019**, *784*, 149.
- [156] N. Hu, X. Lv, Y. Dai, L. Fan, D. Xiong, X. Li, *ACS Appl. Mater. Interfaces* **2018**, *10*, 18665.
- [157] P. Zhu, J. Zang, J. Zhu, Y. Lu, C. Chen, M. Jiang, C. Yan, M. Dirican, R. K. Selvan, D. Kim, *Carbon* **2018**, *126*, 594.
- [158] S. Luo, J. Ruan, Y. Wang, J. Hu, Y. Song, M. Chen, L. Wu, *Small* **2021**, *17*, 2101879.
- [159] R. Saroha, J. Heo, Y. Liu, N. Angulakshmi, Y. Lee, K.-K. Cho, H.-J. Ahn, J.-H. Ahn, *Chem. Eng. J.* **2022**, *431*, 134205.
- [160] K. Xie, K. Yuan, K. Zhang, C. Shen, W. Lv, X. Liu, J.-G. Wang, B. Wei, *ACS Appl. Mater. Interfaces* **2017**, *9*, 4605.
- [161] Y. Ye, L. Wang, L. Guan, F. Wu, J. Qian, T. Zhao, X. Zhang, Y. Xing, J. Shi, L. Li, *Energy Storage Mater.* **2017**, *9*, 126.
- [162] K. Wu, Y. Hu, Z. Cheng, P. Pan, L. Jiang, J. Mao, C. Ni, X. Gu, Z. Wang, *J. Membr. Sci.* **2019**, *592*, 117349.
- [163] M. Li, Y. Wan, J.-K. Huang, A. H. Assen, C.-E. Hsiung, H. Jiang, Y. Han, M. Eddaoudi, Z. Lai, J. Ming, L.-J. Li, *ACS Energy Lett.* **2017**, *2*, 2362.
- [164] P. J. H. Kim, K. Kim, V. G. Pol, *Carbon* **2018**, *131*, 175.
- [165] H. Wu, Y. Huang, S. Xu, W. Zhang, K. Wang, M. Zong, *Chem. Eng. J.* **2017**, *327*, 855.
- [166] D. Wang, Q. Cao, B. Jing, X. Wang, T. Huang, P. Zeng, S. Jiang, Q. Zhang, J. Sun, *Chem. Eng. J.* **2020**, *399*, 125723.
- [167] J. Yang, F. Chen, C. Li, T. Bai, B. Long, X. A. Zhou, *J. Mater. Chem. A* **2016**, *4*, 14324.
- [168] X. Yang, H. Zu, L. Luo, H. Zhang, J. Li, X. Yi, H. Liu, F. Wang, J. Song, *J. Alloys Compd.* **2020**, *833*, 154969.
- [169] S. Jiang, M. Chen, X. Wang, Y. Zhang, C. Huang, Y. Zhang, Y. Wang, *Chem. Eng. J.* **2019**, *355*, 478.
- [170] X. Gu, C. Tong, C. Lai, J. Qiu, X. Huang, W. Yang, B. Wen, L. Liu, Y. Hou, S. Zhang, *J. Mater. Chem. A* **2015**, *3*, 16670.
- [171] L. Wang, Z. Yang, H. Nie, C. Gu, W. Hua, X. Xu, Y. Chen, S. Huang, *J. Mater. Chem. A* **2016**, *4*, 15343.
- [172] J. Yang, L. Xu, S. Li, C. Peng, *Nanoscale* **2020**, *12*, 4645.
- [173] L. Qu, P. Liu, P. Zhang, T. Wang, Y. Yi, P. Yang, X. Tian, M. Li, B. Yang, *Electrochim. Acta* **2019**, *296*, 155.
- [174] M. Chen, X. Zhao, Y. Li, P. Zeng, H. Liu, H. Yu, M. Wu, Z. Li, D. Shao, C. Miao, *Chem. Eng. J.* **2020**, *385*, 123905.
- [175] F. Ma, K. Srinivas, X. Zhang, Z. Zhang, Y. Wu, D. Liu, W. Zhang, Q. Wu, Y. Chen, *Adv. Funct. Mater.* **2022**, *32*, 2206113.
- [176] Z. Huang, S. Wang, X. Guo, J. Safaei, Y. Lei, W.-H. Lai, X. Zhang, B. Sun, D. Shanmukaraj, M. Armand, T. Rojo, G. Wang, *Adv. Mater. Technol.* **2023**, *8*, 2202147.
- [177] S.-D. Seo, C. Choi, D. Park, D.-Y. Lee, S. Park, D.-W. Kim, *Chem. Eng. J.* **2020**, *400*, 125959.
- [178] X. Wu, R. Xie, D. Cai, B. Fei, C. Zhang, Q. Chen, B. Sa, H. Zhan, *Adv. Funct. Mater.* **2024**, *34*, 2315012.
- [179] C. Li, D. Yang, J. Yu, J. Wang, C. Zhang, T. Yang, C. Huang, B. Nan, J. Li, J. Arbiol, Y. Zhou, Q. Zhang, A. Cabot, *Adv. Energy Mater.* **2024**, *14*, 2303551.
- [180] A. K. Das, P. Yadav, T. S. Verma, T. Marulasiddappa, S. Krishnamurty, M. V. Shelke, *ACS Appl. Mater. Interfaces* **2025**, *17*, 7657.
- [181] L. He, K. He, T. Cheng, W. Fang, C. Shang, *Ind. Eng. Chem. Res.* **2025**, *64*, 6034.
- [182] Y. Luo, N. Luo, W. Kong, H. Wu, K. Wang, S. Fan, W. Duan, J. Wang, *Small* **2018**, *14*, 1702853.
- [183] Y. Hu, B. Jin, H. Liu, *Inorg. Chem. Front.* **2025**.

- [184] Y. Fu, Y. Jin, F. Cao, F.-F. Guo, W.-C. Li, B. He, *Ionics* **2025**, *31*, 3243.
- [185] G. Dai, S. Li, M. Shi, L. Sun, Y. Jiang, K. N. Hui, Z. Ye, *Adv. Funct. Mater.* **2024**, *34*, 2315563.
- [186] L. Fang, Z. Feng, L. Cheng, R. E. Winans, T. Li, *Small Methods* **2020**, *4*, 2000315.
- [187] D. Yang, C. Li, M. Sharma, M. Li, J. Wang, J. Wei, K. Liu, Y. Zhang, J. Li, G. Henkelman, *Energy Storage Mater.* **2024**, *66*, 103240.
- [188] F. Wang, J. Li, J. Zhao, Y. Yang, C. Su, Y. L. Zhong, Q.-H. Yang, J. Lu, *ACS Mater. Lett.* **2020**, *2*, 1450.
- [189] L. Zhong, L. Zhang, S. Li, *ACS Mater. Lett.* **2021**, *3*, 110.
- [190] F.-J. Lin, C.-L. Huang, X.-Y. Jiang, J.-Q. Liao, Y.-Y. Li, *ACS Sustainable Chem. Eng.* **2024**, *12*, 3478.
- [191] M. Zhang, S. Kong, B. Chen, M. Wu, *Batteries* **2023**, *10*, 15.
- [192] D. N. Buckley, C. O'Dwyer, N. Quill, R. P. Lynch, in *Energy Storage Options and Their Environmental Impact* (Eds: R. E. Hester, R. M. Harrison), The Royal Society of Chemistry **2018**, pp. 115–149.
- [193] P. Zhu, J. Zhu, J. Zang, C. Chen, Y. Lu, M. Jiang, C. Yan, M. Dirican, R. K. Selvan, X. Zhang, *J. Mater. Chem. A* **2017**, *5*, 15096.
- [194] X. Gu, C. Lai, F. Liu, W. Yang, Y. Hou, S. Zhang, *J. Mater. Chem. A* **2015**, *3*, 9502.
- [195] X. Wang, Z. Wang, L. Chen, *J. Power Sources* **2013**, *242*, 65.
- [196] Y. Liu, X. Qin, S. Zhang, G. Liang, F. Kang, G. Chen, B. Li, *ACS Appl. Mater. Interfaces* **2018**, *10*, 26264.
- [197] Y.-S. Su, A. Manthiram, *Nat. Commun.* **2012**, *3*, 1166.
- [198] X. Xiang, J. Y. Wu, Q. X. Shi, Q. Xia, Z. G. Xue, X. L. Xie, Y. S. Ye, *J. Mater. Chem. A* **2019**, *7*, 9110.
- [199] M. Liu, Q. Li, X. Qin, G. Liang, W. Han, D. Zhou, Y. He, B. Li, F. Kang, *Small* **2017**, *13*, 1602539.
- [200] Y. Zhou, C. Zhou, Q. Li, C. Yan, B. Han, K. Xia, Q. Gao, J. Wu, *Adv. Mater.* **2015**, *27*, 3774.
- [201] S. Pan, Z. Yin, Q. Cheng, G. Zhang, X. Yu, Z. Pan, H. Rao, X. Zhong, *J. Alloys Compd.* **2020**, *832*, 154947.
- [202] X. Li, L. Chu, Y. Wang, L. Pan, *Mater. Sci. Eng. B* **2016**, *205*, 46.
- [203] Z. Sun, J. Zhang, L. Yin, G. Hu, R. Fang, H.-M. Cheng, F. Li, *Nat. Commun.* **2017**, *8*, 14627.
- [204] W. Ge, L. Wang, C. Li, C. Wang, D. Wang, Y. Qian, L. Xu, *J. Mater. Chem. A* **2020**, *8*, 6276.

Manuscript received: March 24, 2025

Revised manuscript received: June 4, 2025

Version of record online: